Chemical Geology, 106 (1993) 77–101
Elsevier Science Publishers B.V., Amsterdam

[AL]

Formation and transformation processes of iron duricrust systems in tropical humid environment

A. Beauvais[a] and F. Colin[b]

[a]*ORSTOM and Laboratoire de Pétrologie de la Surface, Université de Poitiers, F-86022 Poitiers Cedex, France*
[b]*ORSTOM and U.M. GECO, Université Aix-Marseille III, F-13397 Marseille Cedex 13, France*

(Received June 30, 1991; revised and accepted October 20, 1992)

ABSTRACT

Beauvais, A. and Colin, F., 1993. Formation and transformation processes of iron duricrust systems in tropical humid environment. Chem. Geol., 106: 77–101.

Formation and transformation processes of iron duricrust developed under tropical humid conditions in the southeastern part of the Central African Republic have been investigated in terms of geomorphological, petrological and geochemical pathways. The study of five typical weathering profiles of the most extensive iron duricrust system now known in the world indicates that saprolitization and ferruginization are sequentially involved in such processes, as reflected by kaolinite–gibbsite and hematite–goethite replacements. Alkali earths, rare earths, metals and elements belonging to chemically inert minerals segregate during saprolite and iron duricrust formation and degradation. Mass-balance calculations performed on a typical weathering system enable us to quantify net mass element transfers deriving from lateritic weathering processes. Volumetric change, collapse or dilation, as well as Al and Ti clearly discriminate between the saprolitization and ferruginization processes. Saprolite development preserves the geochemical inheritance of parent rocks, whereas ferruginization depletes it and mostly reflects, through mineralogical pathways, pedoclimatic conditions and global climatic changes. The global iron duricrust system of the southern part of Central Africa derived from previous hematite-rich crust, and not from ancient bauxites as it is generally believed for iron crusts, formed on West African shields.

1. Introduction

The global lateritic weathering mantle covers one-third of the emerged continental areas of the world (Nahon, 1986). In tropical areas, the surficial part of this mantle consists of an iron duricrust reaching up to 10 m in thickness. Most of the studies performed in Africa on lateritic systems addressed the iron duricrust formed either under tropical contrasted climate (Maignien, 1958; Grandin, 1973; Boulet, 1974; Nahon, 1976; Leprun, 1979; Ambrosi, 1984) or under humid equatorial climate conditions (Martin, 1966; Novikoff, 1974; Martin et al., 1981; D. Muller et al., 1981; J.P. Muller and Bocquier, 1986; J.P. Muller, 1987; Colin et al., 1989). These authors have investigated the iron duricrust either in terms of geomorphological distribution at a large scale, or in terms of petrological differentiation at the scale of profiles and minerals, and recently in terms of geochemical pathways at the scale of the landscape (Davies and Bloxham, 1979; Matheis, 1981; Butt, 1987; Colin et al., 1989; Freyssinet et al., 1989; Lecomte and Colin, 1989; Roquin et al., 1989; Colin and Vieillard, 1991). Considering that each investigation method has to be applied together to the whole system, we propose here to globally study the iron duricrust systems of the Central Africa Republic (R.C.A.) which are the most extensive iron duricrust known at present in the world (Boulvert, 1976, 1983; Beauvais and Mazaltarim, 1988). Our investigations were

conducted in the Dembia–Zemio area, southeastern Central Africa, where iron duricrusts evolve today under tropical humid conditions.

The purpose of this paper is to qualitatively and quantitatively explain the weathering processes leading to the formation and transformation of iron duricrust systems by combining geomorphological and petrological observations, with calculation of net mass element transfers and volume changes caused by these processes.

2. Geographic and geologic setting

The Dembia–Zemio area is located in the southeastern part of the R.C.A. (Fig. 1). This area corresponds to a transitional climatic domain between the humid equatorial zone of the intracratonic Congolese basin and the tropical contrasted climate of the intracratonic Tchadian basin. The climate is humid tropical with a dry season extending from December to February. The mean annual rainfall is ~1600 mm, the mean annual temperature is 25°C and the mean relative humidity is 80%.

The landscape consists of plateaus ranging from 600 to 650 m above mean sea level (a.s.l.) in elevation and of weakly inclined slopes cut out by straight and deep thalwegs. The vegetation consists of a patchwork of: (1) humid (valleys) or semi-humid (slopes and plateaus) forests; and (2) of savanna (slopes and plateaus) accounting for (1) 10%, 10.6% and (2) 79.4%, respectively (Fig. 1).

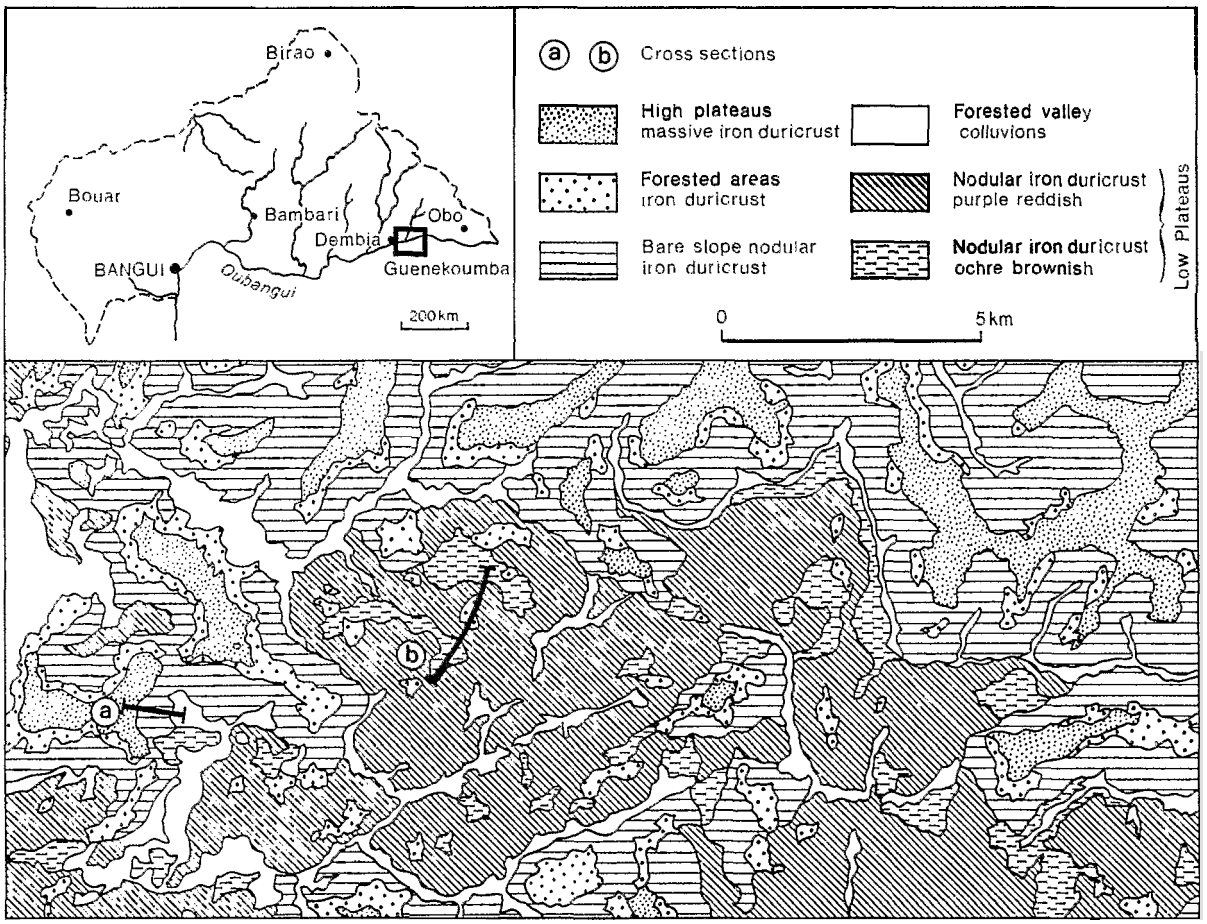

Fig. 1. Geographical setting of the Dembia–Zemio area and spatial relationship between surficial layers.

The fresh rocks have been observed when outcropping in rivers. Previous regional mappings report that the bedrock consists of a Barrimian amphibolitic–pyroxenitic complex (Mestraud, 1982; Poidevin, 1991). The few collected fresh rocks are amphibolo-schists.

3. Methods

According to the geomorphological study of the area (250 km^2), representative sequences were selected (Fig. 1) and 44 pits were dug from the surface to the water table, which however does not permit to observe the parent rock. After careful macroscopic description of each layer, five typical weathering profiles were chosen as representative of the whole set (Fig. 2). Oriented samples were gathered within each layer in order to study thin sections and bulk samples by means of photonic and scanning electron microscopic (SEM), X-ray diffractometer (XRD), and inductively coupled plasma spectrometer (ICP) chemical analyses. ICP analysis was used to quantify major elements (given in wt%) such as SiO_2 (detection limit at 5 ppm), Al_2O_3 (20 ppm), Fe_2O_3, MgO (0.5 ppm), CaO (0.5 ppm), Na_2O (100 ppm), K_2O (100 ppm), MnO (0.5 ppm), TiO_2 (5 ppm) and P_2O_5 (1000 ppm), and trace elements (given in ppm) such as Sr (detection limit at 0.5 ppm), Ba (0.5 ppm), V (1 ppm), Ni (5 ppm), Co (2 ppm), Cr (2 ppm), Zn (2 ppm), Cu (1 ppm), Sc (0.2 ppm), Y (0.5 ppm), Zr (2 ppm), La (5 ppm), Ce (20 ppm), Eu (2 ppm), Yb (0.2 ppm), Lu (0.1 ppm) and Nb (10 ppm). Elements for which concentrations are below the detection limit (Ca, Na, K, Eu) are not taken into account.

The mineralogical composition of the rocks was quantified by the mathematical method established by Mazaltarim (1989): semi-quantitative XRD results are corrected by normative calculations based on chemical analyses of SiO_2, Al_2O_3, Fe_2O_3 and H_2O (loss on ignition at 1000°C), in order to evaluate the proportions of kaolinite, goethite, hematite, gibbsite and quartz.

Factor analysis was carried out on mineralogical and chemical data using the SAS (1985) software package. The statistical analysis proceeds in four steps: (1) computation of the correlation matrix for the variables, application of the Bartlett test of sphericity to evaluate the appropriateness of the factor model, and measurement of sampling adequacy of variables; (2) extraction of eigenvectors and eigenvalues from the correlation matrix using the maximum-likehood extraction technique (Lebart et al., 1979); (3) application of the Varimax–rotation procedure; (4) computation of factor scores which give the load of each sample with respect to the extracted factors. The aim of the statistical analysis is to identify chemical and mineralogical associations. The factor scores obtained allow the validity location of the samples corresponding to a given mineralogical–chemical relationship. The systematics of the data was then confirmed by petrological study. Such statistical analysis has recently been clearly demonstrated to be a useful mathematical tool applied to soil and global weathering system study (Litaor et al., 1989; Boski and Herbosch, 1990; Roquin et al., 1990; Donkin and Fey, 1991; De Carlo and McMurtry, 1992) after the well-documented discussion carried out by Jöreskog et al. (1976) on the subject of the statistical analysis of geological data.

Interpretation of mass transfer during weathering requires the application of rigorous means of calculating losses or gains based on thorough petrological study (Colin et al., 1992). Formal mass-balance equations in which w and p subscripts refer to weathered and parent rocks, respectively, as established by Brimhall et al. (1988) are functional forms of constitutive relationships between weathered material chemical composition, bulk density, porosity and volume change in relation to corresponding chemical and physical properties of fresh parent rocks. Measurements of

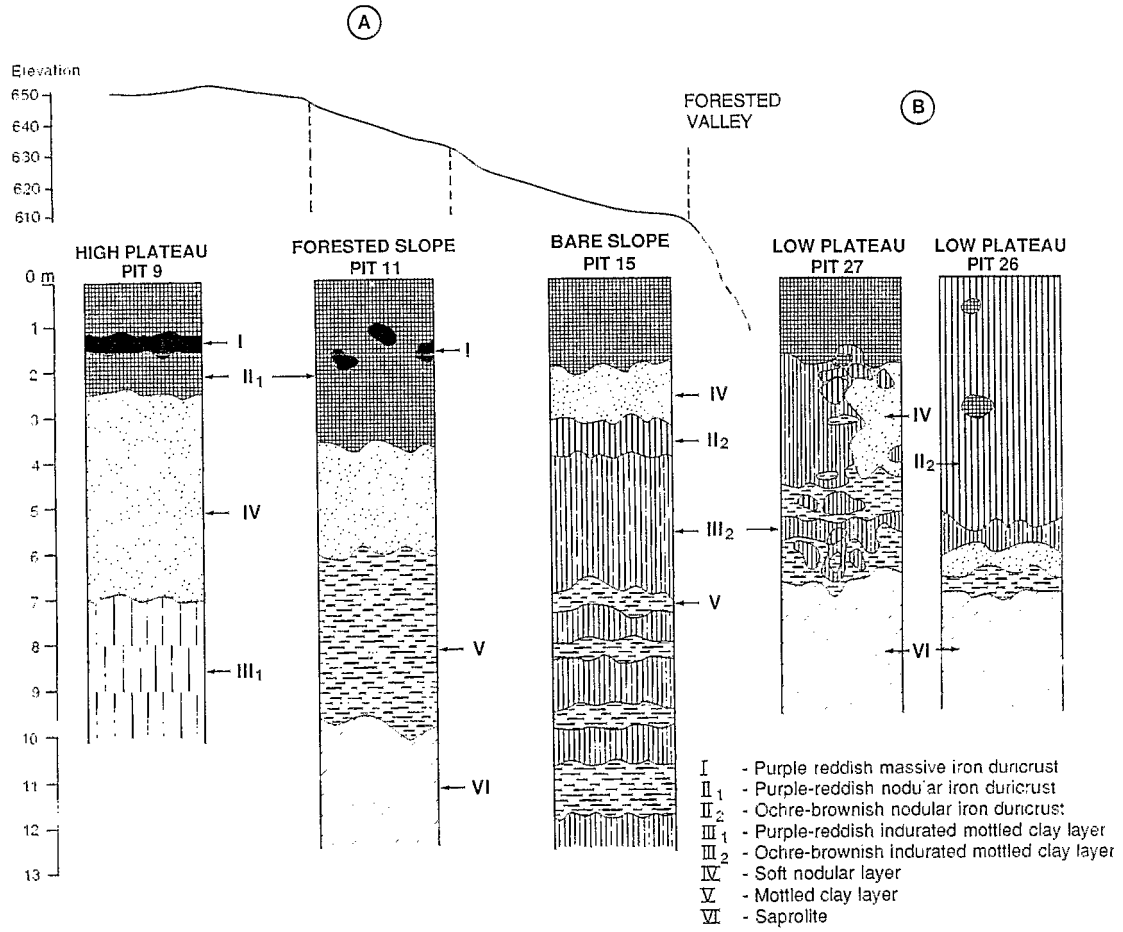

Fig. 2. Sketch of weathering type-profiles corresponding to the *a* and *b* cross-sections in Fig. 1 (I = massive iron duricrust; II_1 = purple-reddish nodular iron duricrust; II_2 = ochre-brownish or vermiform iron duricrust; III_1 = purple-reddish indurated mottled clay layer; III_2 = ochre-brownish indurated mottled clay layer; IV = soft nodular layer; V = mottled clay layer; VI = saprolite).

bulk density (ρ_w) were made on rock samples after drying by weighing and coating them with molten paraffin wax, followed by immersion in water to measure their displaced volume. Bulk density was measured with an accuracy of $\sim \pm 1\%$. Grain density (ρ_g) was measured by water picnometer with an accuracy of $\sim \pm 1\%$. Porosity was calculated from the following equation:

$$(\text{porosity}) = \phi = 1 - \rho_w/\rho_g \qquad (1)$$

Volumetric change is defined by:

$$\epsilon_{i,w} = \frac{\rho_p}{\rho_w}\frac{C_{i,p}}{C_{i,w}} - 1 \qquad (2)$$

where the subscript i pertains to an element considered to be immobile during weathering; ρ is the bulk density in g cm^{-3}; and C is the concentration in g/100 g.

Extraction or addition of a chemical mobile element j either by solute migration or physical translocation is quantified by the open-system mass-transport function ($\tau_{j,w}$) defined by:

$$\tau_{j,w} = \frac{\rho_w}{\rho_p}\frac{C_{j,w}}{C_{j,p}}(\epsilon_{i,w} + 1) - 1 \qquad (3)$$

Mass-balance equations were applied to a typical weathering system (pit 11, see Fig. 2)

in order to quantify the net mass gains and losses of elements during conversion of parent rock into weathered materials through lateritic weathering processes at present day and during past periods. We chose this particular profile because it was the most complete one in terms of representative weathered rock samples and it was the only place where saprolite was found. These facts enabled us to genetically link the weathered rocks to neighbouring outcropping fresh greenschist formations.

SEM observations have shown that zircons extracted from this profile are of crystalline habits and not significantly affected by dissolution (in contrast to other heavy minerals such as ilmenite), therefore we use Zr as the immobile index *i* in our system.

4. Spatial distribution, petrographical and mineralogical patterns of the lateritic weathering systems

Three iron duricrust systems can be spatially and petrologically distinguished on: high plateaus (*1*), slopes (*2*) and low plateaus (*3*) (Figs. 1 and 2). This is in agreement with previous observations done at the 1000-km^2 regional scale (Beauvais and Mazaltharim, 1988).

4.1. The high plateau system (1)

The ferruginous iron duricrust is 3 m thick and exhibits a massive (I) or nodular (II_1) structure (Fig. 2). The massive iron duricrust is purple reddish [10R *3/5*, Munsell® (1954) color chart]. It is composed of an indurated ferruginous matrix which is rich in hematite and kaolinite booklets of 100–200 μm in length. Kaolinite derives from pseudomorphic weathering of micas (Fig. 3-1). These booklets consist of alternative ferruginous and non-ferruginous sheets, without epigenetic replacement of kaolinite by hematite.

The nodular iron duricrust (II_1) consists of purple-reddish centimeters-length nodules surrounded by a brown millimeters-thick rim. The core of the nodule is hematitic, while the outer part, centripetally developed at the expense of the core is goethitic as it has been already observed by Nahon (1976) in iron duricrust profiles of Ndias (Senegal). This microscopic transformation develops also at the scale of the profile where goethite-rich nodular iron duricrusts form from the hematite-rich massive duricrust blocks.

The soft nodular layer (IV) is 5–7 m thick and contains centimeters-long hematitic nodules surrounded by a micro-aggregated ferruginous clayey matrix. These nodules have an elongated shape and they lay within the layer with their great axis horizontal. They are purple reddish and have a fine-bedded structure, which is inherited from the parental rock. They are made of hematite coexisting with numerous small kaolinite crystallites (Fig. 3-2 and -3). A few polyhedric nodules, with irregular and rough edges are scattered within the matrix of the upper part of the nodular layer. A goethitic rim develops at the expense of the hematitic core, reflecting the centripetal transformation seen within the overlying iron duricrust. Clayey nodule-depleted domains occur at the top of the layer. They are crossed by numerous biological channels of centimetric size (termites, roots, etc.). At the lower part, soft purple-reddish mottled spots remain within the microaggregated matrix and preserve the microbedded structure inherited from the parent rock.

The mottled clay layer is differentiated from 7 m deep into an upper indurated compartment located above the water table and a lower one under the water table. It consists of coalescent ferruginous nodules which constitute coherent volumes similar to the purple-reddish indurated mottled clay called elsewhere by Herbillon and Nahon (1988) "soft iron duricrust". Both coherent volumes and surrounding matrix are crosscut by a brown goethitic network. Furthermore, at the level of water table fluctuation, lithiophorite with cerianite co-

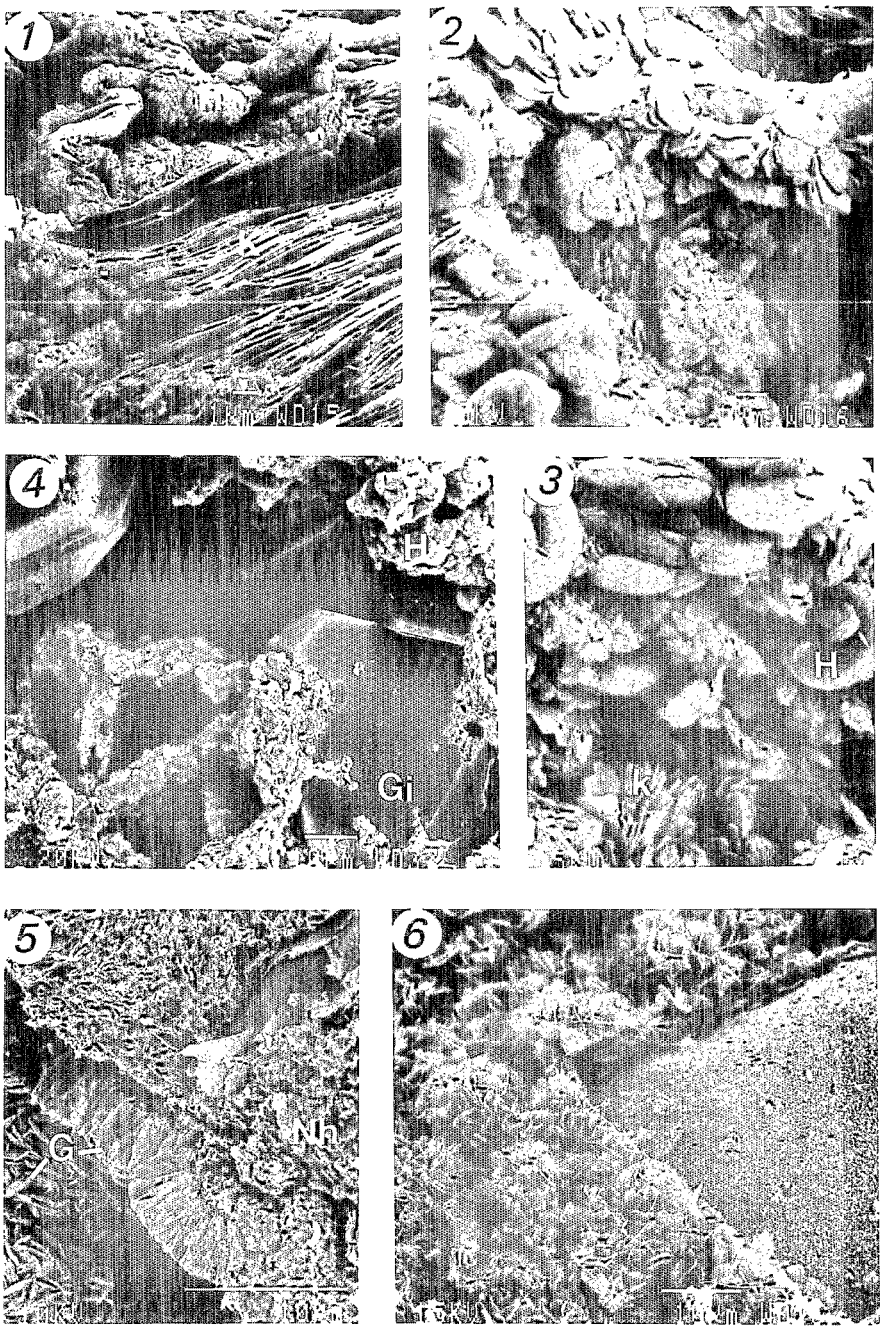

Fig. 3. SEM micrographs of iron duricrust and soft nodular layers. *1*=massive iron duricrust of high-plateau profile (*H*=hematite, *K*=kaolinite booklet); *2*, *3*=soft nodular layer of high-plateau profile (*H*=hematite, *k*=kaolinite crystallite); *4*=nodular iron duricrust of forested slope profile (*Gi*=gibbsite crystal, *H*=hematite); *5*=nodular iron duricrust of the bare slope profile (*G*=cortex of goethite, *Nh*=hematitic nodule); *6*=lithiophorite in indurated mottled clay layer of the bare slope profile.

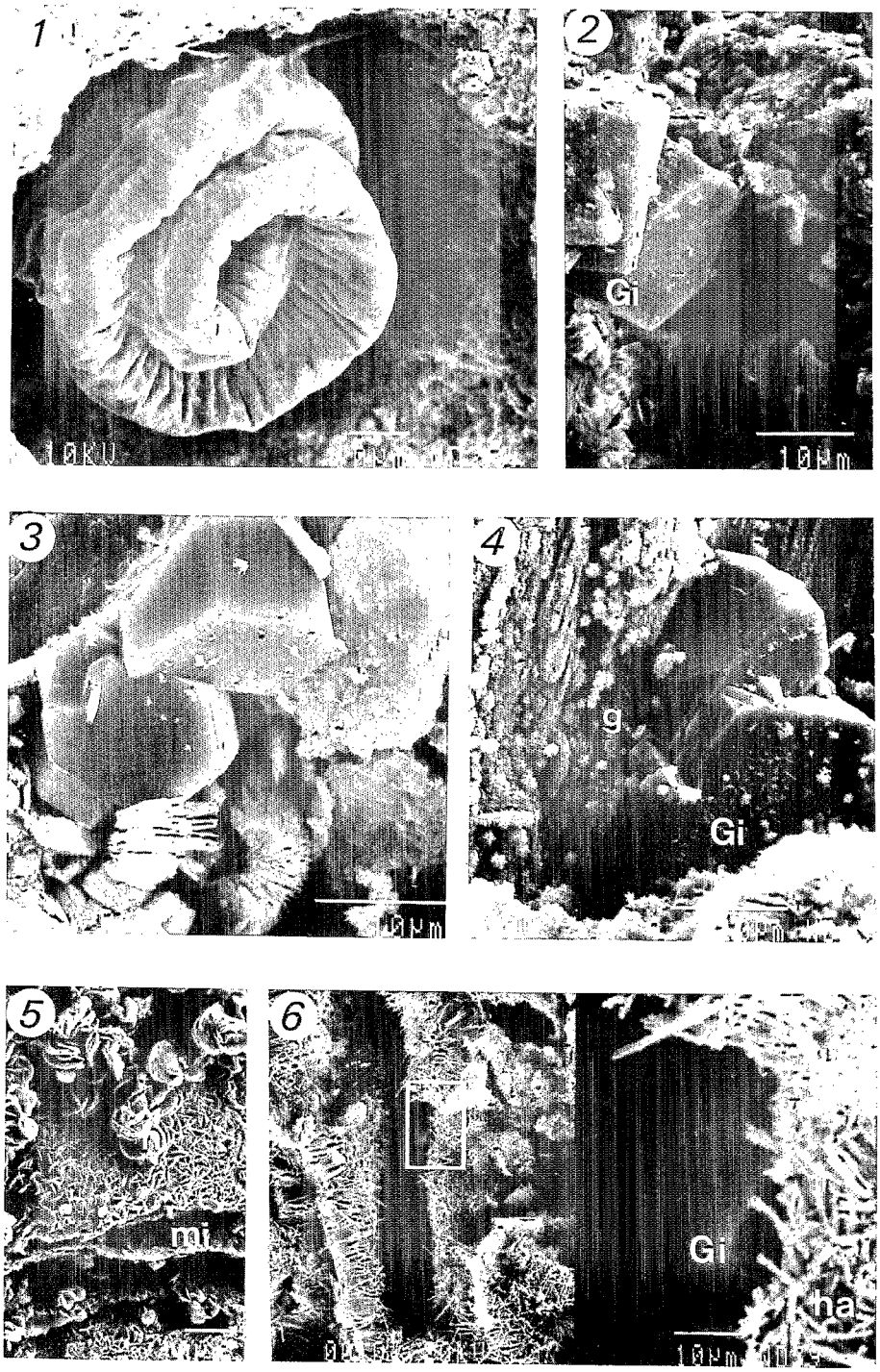

Fig. 4. SEM micrographs of mottled clay layer and saprolite of forested slope profile. *1*, *2*=biological figure of pedoturbation and gibbsite formation in the upper part of the mottled clay layer; *3*, *4*, *5*, *6*=upper part of the saprolite (*g*=goethite, *Gi*=gibbsite crystals, *h*=hematite, *mi*=relict mica, *ha*=halloysite).

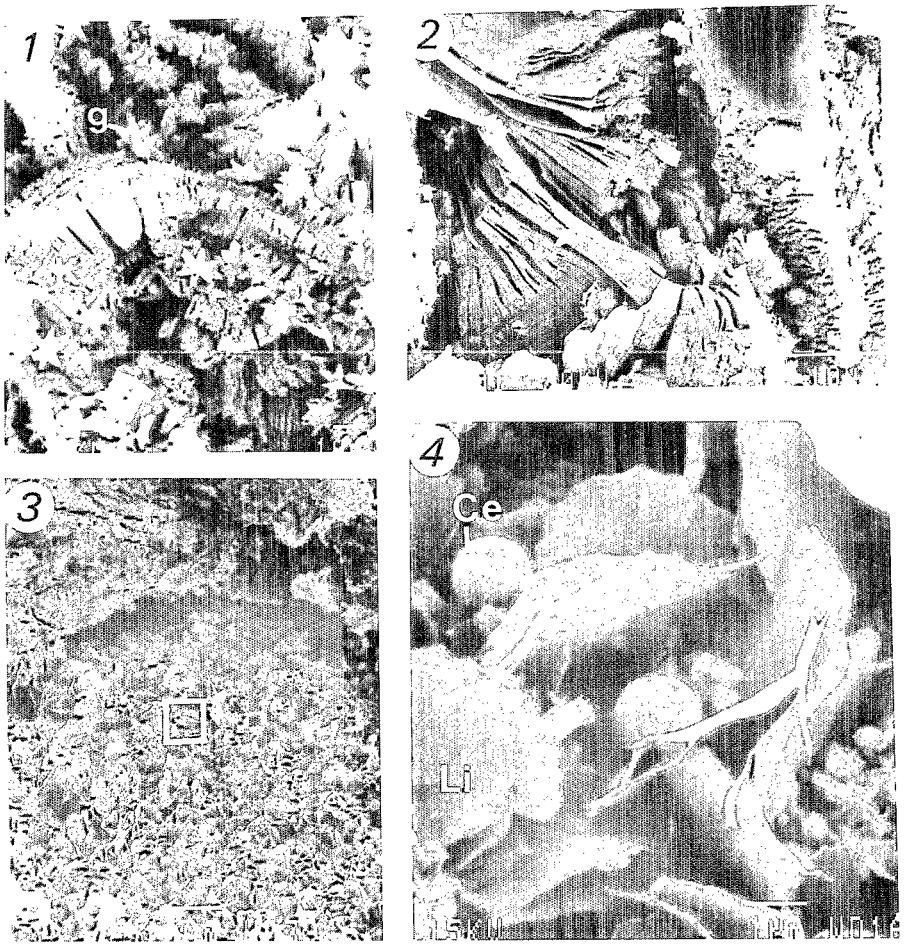

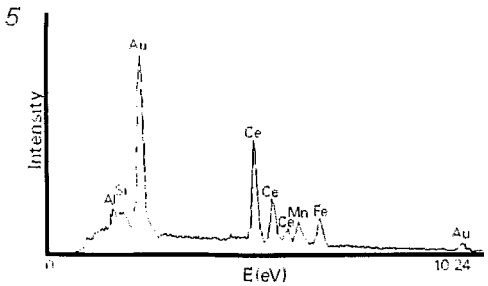

Fig. 5. SEM micrographs of saprolite and indurated mottled clay layer. *1*=lower part of the saprolite (*g*=goethite, *K*=kaolinite booklet); *2*=details of kaolinite booklets which derives from pseudomorphic weathering of parent minerals as micas and amphiboles; *3*, *4*=indurated mottled clay layer at the base of the high-plateau profile (*Ce*=cerianite micropisolite, *Li*=lithiophorite); *5*=Tracor® semi-quantitative analysis of cerianite–lithiophorite habitus.

precipitation is observed under the SEM (see Fig. 5-3, -4 and -5).

4.2. The slope system (2)

The slope of the high plateau varies in elevation from 645 to 600 m a.s.l. The slope system is divided into an upslope forested subsystem and a downslope bare one, separated by a meters-large scarp. The forested part is concave and inclines 10°, whereas the bare part inclines 5°.

According to this differentiation, two profiles were considered (Fig. 2). These weathering profiles consist of a nodular iron duricrust which presents a purple-reddish (II_1) or ochre-brownish (II_2) color, a soft nodular layer (IV),

an indurated mottled clay layer (III_2), a mottled clay layer (V) and a saprolite (VI). The profile of the forested part evolves under the influence of high biological activity (roots, termites, burrowing animals, etc.).

The purple-reddish nodular iron duricrust (II_1) is 2–3 m thick and has a nodular structure with a few millimeters-large vacuoles. It consists of numerous centimeters-long hematitic gibbsitic purple-reddish nodules (Fig. 3-4) outlined by a fine goethitic cortex (Fig. 3-5) and, at the macroscopic scale, a few massive blocks as remnants of the plateau iron duricrust. Under the photonic microscope, the ilmenite shows partial dissolution features.

The ochre-brownish nodular iron duricrust (II_2) is 0.7 m thick and is located between the soft nodular layer and the indurated mottled clay layer in the downslope profile. It consists of a few centimeters-length diffuse hematitic nodules scattered within an ochre-brown goethitic matrix. Both these iron duricrust types contain a few quartz grains of a few millimeters in diameter. This iron duricrust is petrographically similar to the vermiform laterite observed by McFarlane (1976) in weathering profiles of Uganda.

The soft nodular layer (IV) is 2–3 m thick in the forested part and 1 m thick in the bare one. It consists mainly of a red-yellow sandy–clayey matrix containing hematitic centimeter-long nodules. These nodules are petrographically similar to those observed in the soft nodular layer of the high plateau system, but they contain numerous gibbsite crystals. Therefore, the polyhedric nodules are here more numerous than the elongated ones.

The indurated mottled clay layer (III_2) is 8 m thick and occurs only in the downslope subsystem. It consists of ochre or brown (7.5 YR *7/6*) centimeters-thick ferruginous domains, crosscut by centimeter-thick vertically oriented tubules in which lithiophorite precipitates as a secondary phase (Fig. 3-6). These tubules originate from disferruginization processes and are filled with a kaolinitic white matrix containing small residual quartz crystals.

The mottled clay layer (V) is 4 m thick within the upslope profile and occurs as scattered decimeter-elongated lenses within the indurated mottled clay layer of the downslope profile. Upslope, this layer consists of a ferruginous clay matrix and of a clay matrix spotted by white-yellow to red-orange centimeter-thick domains. Intense bio-pedoturbation processes affect the matrices (Fig. 4-1) and lead to increasing pore-size development and gibbsite formation (Fig. 4-2). The upper part of the layer was derived from ferruginization of the clay matrix, and thus it appears more ferruginous than the base of layer. Within the lower part of the downslope profile, kaolinite and goethite form a white-yellow mottled clay matrix.

The saprolite (VI) occurs at a depth of 10 m in the upslope profile (Fig. 2) and exhibits a fine-bedded structure which reflects the initial structure of the parent rock. The upper part consists of an ochre gibbsitic matrix (Fig. 4-3), exhibiting numerous bio-pedoturbation outlines, and which contains millimeters-thick goethitic or hematitic spots (Fig. 4-4) developing on relict micas (Fig. 4-5). The gibbsite often crystallizes within large pores ($> 10\,\mu m$) from halloysite-rich domains (Fig. 4-6). The tubular needles of halloysite have grown perpendicular to kaolinite weathered-mica sheets (Fig. 4-6).

The lower part bears yellow kaolinitic matrix including millimeters-thick diffuse goethitic domains (Fig. 5-1). Kaolinite forms booklets which result from the pseudomorphic replacement of the parent minerals (Fig. 5-2). A network of millimeters-thick cracks filled with kaolinite crosscut the matrix. Some supergene heavy minerals such as anatase are precipitated within the pores.

4.3. The low plateau system (3)

The low plateaus are flat or convex and culminate at 600 m a.s.l. They are connected to

the high plateaus by thalwegs and slopes (Fig. 1).

Two weathering profiles are representative of this system (Fig. 2). They consist from the top to the base of an iron duricrust (II_1 and II_2), an indurated mottled clay layer (III_2), a soft nodular layer (IV), a mottled clay layer (V) and a saprolite (VI).

The iron duricrust is ~5 m thick and consists of a purple-reddish nodular formation (II_1) and an ochre-brownish (7.5 YR 5/5) nodular formation (II_2), both tightly overlapped and similar to the duricrusts of the bare slope profile (Fig. 2). The ochre-brownish nodular duricrust is the most goethite–kaolinite–quartz-rich duricrust of the three systems.

The indurated mottled clay layer (III_2) is 3 m thick and its constituents are mineralogically similar to those which form the indurated mottled clay layer of the bare slope profile.

The soft nodular layer (IV) is 0.5–3 m thick (Fig. 2). Within this layer, centimeter-long hematitic and goethitic polyhedric nodules are spread out all over through a ferruginous clayey matrix spotted by millimeter-thick kaolinitic white-yellow domains.

The mottled clay layer (V) is 0.5–1.5 m thick and is composed of a kaolinitic and goethitic matrix including centimeter-long hematitic soft elongated nodules which have a fine-bedded structure and are obliquely oriented.

The saprolite (VI) occurs at a depth of 7 m and consists of a yellow sandy–clayey kaolinitic–goethitic matrix with disseminated centimeter-thick kaolinite–quartz-rich domains. This saprolite is Fe-depleted and quartz-rich compared to the saprolite of the other system.

These significant observations allow us to draw partial conclusions concerning the vertical and lateral relationships between the three systems.

A given system is characterized by petrographical features which qualify material inherited from another system or specific material formed in situ. This is illustrated by:

(1) The occurrence of an indurated goethitic mottled clay layer at the base of the soft nodular layer within the high-plateau profile, which predates the iron duricrust of the slope system.

(2) The remnants of massive iron duricrust within the slope nodular iron duricrust derived from the high plateau system.

(3) The presence of a thick indurated goethitic mottled clay layer within the bare slope profile similar to the iron duricrust of the low plateaus.

(4) The soft nodular layers contain two populations of nodules: the elongated nodules preserving the parental fine-bedded structure called lithomorphous by Beauvais (1989) and the polyhedric ones with a pedogenetic structure called argillomorphous in Senegalese iron duricrust by Nahon (1976). Goethitic cortex developing from hematitic cores results from hydratation processes of hematitic nodules either derived from overlying nodular iron duricrust or formed in situ. The base of soft nodular layer of the high-plateau profile is indurated, and a paragenesis of lithiophorite and cerianite was observed. This well indicates an oxidizing microenvironment, which promotes the actual development of a goethite-rich iron duricrust.

(5) Kaolinitic domains in the saprolite preserve the initial structure of the parent rock. In contrast, gibbsitic domains have pedoturbated structure which has been also observed in other areas (Boulangé, 1983; J.P. Muller, 1987; Lucas, 1989). Bocquier et al. (1983) described the pseudomorphic weathering of micas in halloysite, followed by kaolinite in the latest stage. Here, halloysite develops by hydratation of kaolinite, and grows perpendicularly to larges pores. Furthermore, gibbsite crystallizes from halloysite in a final stage, and anatase secondary forms in these sites.

Vertical and lateral evolution of the three systems transform the parent rock into iron duricrust through the intermediate and transitional processes of kaolinitization–gibbsitization (saprolite) and hematitization–goethitization (upper layers) processes.

5. Saprolitization and ferruginization development

5.1. Quantitative relationships between mineralogy and bulk chemistry

5.1.1. Within the saprolite. The saprolite of the forested and low-plateau profiles is strongly differentiated in terms of mineralogy and bulk chemistry (Table 1; Fig. 6).

The saprolite of the forested slope is richest in gibbsite (23.5 g/100 cm^3) and in Fe_2O_3 (44.8 g/100 cm^3), which manifests goethite occurrences (51.5 g/100 cm^3).

The saprolite of the low plateau is richest in silica (61.5 g/100 cm^3) and in alumina (43 g/100 cm^3), which reflects quartz (11.6 g/100 cm^3) and kaolinite (113 g/100 cm^3) contents.

The trace-element signatures clearly identify the saprolite layers. Transition elements such as Mn, V, Ni, Co, Cr and Cu have high contents in the forested slope saprolite, whereas the alkaline earths such as Sr, Ba and the rare-earth elements such as La, Ce, and also Y and Zr concentrate in the low-plateau saprolite (Fig. 6).

5.1.2. Within the indurated mottled clay layers. The mottled clay layers are mineralogically and chemically transitional between the underlying saprolites and the overlying soft nodular layers.

The high-plateau indurated mottled clay layer is richest in Fe (161.6 g/100 cm^3) and goethite (156 g/100 cm^3) (Table 2). The bare slope layer is characterized by high silica and alumina contents (52.4 and 46.2 g/100 cm^3, respectively), reflected in the amount of kaolinite (117.2 g/100 cm^3). The low-plateau layer is the richest in quartz (11.5 g/100 cm^3) and in hematite (20.7 g/100 cm^3).

5.1.3. Within the soft nodular layers. In contrast to saprolite, the soft nodular layers are not clearly characterized by their mineralogy and bulk chemistry. Only slight differences can be noticed (Table 3).

The high-plateau layer is, on average, the richest in Fe (116.4 g/100 cm^3) as well as hematite (70.9 g/100 cm^3) and kaolinite (116 g/100 cm^3) (Table 3). In its upper part, it is further characterized by an Fe-depleted layer (77.3 g/100 cm^3) rich in kaolinite (148 g/100 cm^3) (Table 4). On the other hand, the base of the high-plateau profile is made up of an Fe-rich (161.6 g/100 cm^3) goethitic layer (156 g/100 cm^3). In comparison with the iron duricrusts (Table 5), this layer is the most ferruginous and richest in goethite.

The forested slope layer is the richest in goethite (74 g/100 cm^3), whereas the bare slope layer has the highest content of alumina with 56.5 g/100 cm^3, reflecting gibbsite (46.4 g/100 cm^3) occurrence (Table 3).

The low-plateau layer is the richest in silica with 51.4 g/100 cm^3, reflecting the amount of quartz (15.4 g/cm^3).

TABLE 1

Bulk chemical and mineralogical average composition of saprolites of each system expressed in gram per 100 cm^3 of sample

System	*n*	*d*	SiO_2	Al_2O_3	Fe_2O_3	Mn_3O_4	MgO	K_2O	TiO_2	P_2O_5	H_2O	Total	Q	K	G	H	Gi	Total
1	7	1.47	32	42.3	44.8	0.2	0.09	0	4.7	0.4	21.6	146.1	0	72	51.5	0	23.5	147
3	5	1.45	61.5	43.1	18.3	0.14	0.06	0.1	5.3	0.3	15.6	144.4	11.6	113	17.4	3	0	145

1=forested slope profile; *3*=low-plateau profile; *n*=number of samples; *d*=bulk density; Q=quartz; K=kaolinite; G=goethite; H=hematite; Gi=gibbsite.

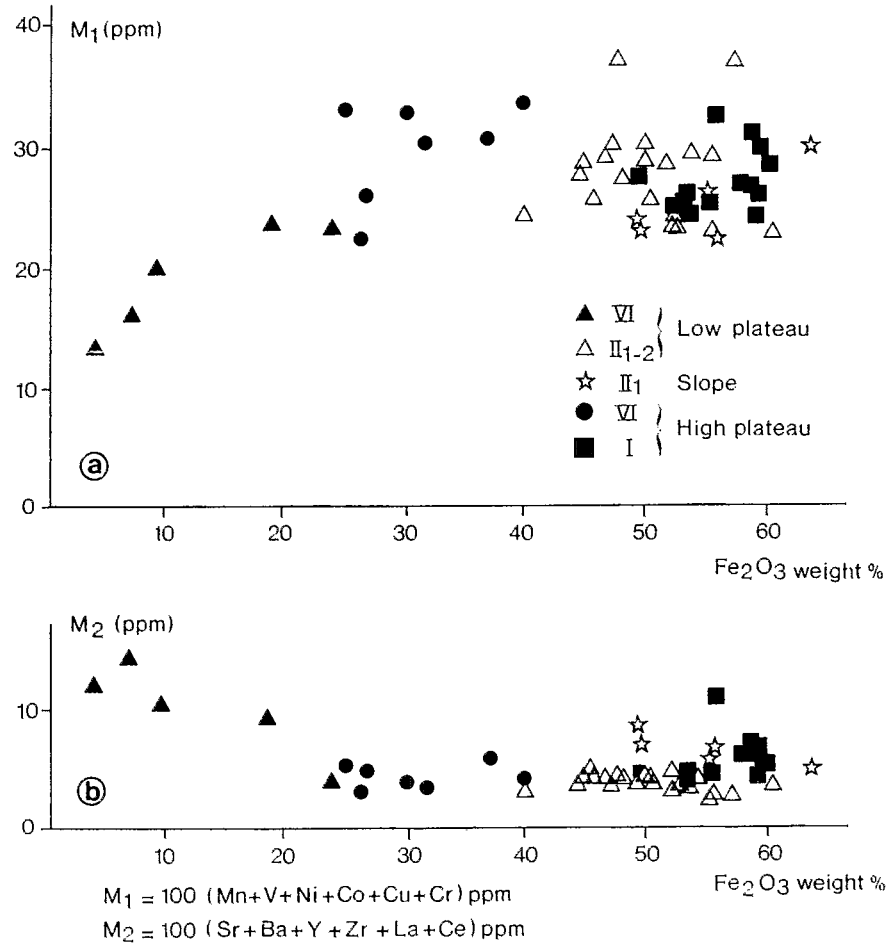

Fig. 6. Trace-element contents of saprolites compared to iron duricrusts: (a) $M_1=100(Mn+V+Ni+Co+Cu+Cr)$ vs. Fe_2O_3; and (b) $M_2=100(Sr+Ba+Y+Zr+La+Ce)$ vs. Fe_2O_3.

TABLE 2

Bulk chemical and mineralogical average composition of indurated mottled clay layer (III) of each system expressed in gram per 100 cm^3 of sample

System	n	d	SiO_2	Al_2O_3	Fe_2O_3	Mn_3O_4	MgO	K_2O	TiO_2	P_2O_5	H_2O	Total	Q	K	G	H	Gi	Total
1	2	2.65	27.8	36.3	161.6	0.1	0.1	0	4.9	2.4	32	265.2	5	87.5	156	10.6	0	259.1
2	8	2.02	52.4	46.2	71.2	0.22	0.12	0	6.1	0.97	24.6	201.8	6	117.2	68.7	10.1	0	202
3	6	2.3	40.2	40.5	114.4	0.16	0.09	0.16	4.1	1	27.2	227.9	11.5	98.9	98.9	20.7	0	230

1=high-plateau profile; *2*=bare slope profile; *3*=low-plateau profile; n=number of samples; d=bulk density; Q=quartz; K=kaolinite; G=goethite; H=hematite; Gi=gibbsite.

5.1.4. Within the iron duricrust. The mineralogical composition of the varied iron duricrust is a more efficient signature than the bulk chemistry (Table 5; Fig. 6).

The high kaolinite and goethite contents (97.5 and 115 g/100 cm^3, respectively) characterize the low-plateau ochre-brownish nodular duricrust, whereas gibbsite (57 g/100 cm^3) and hematite (106 g/100 cm^3) are the main components of the purple-reddish nodu-

TABLE 3

Bulk chemical and mineralogical average composition of soft nodular layer (IV) of each system expressed in gram per 100 cm^3 of sample

System	n	d	SiO_2	Al_2O_3	Fe_2O_3	Mn_3O_4	MgO	K_2O	TiO_2	P_2O_5	H_2O	Total	Q	K	G	H	Gi	Total
*1*a	3	2.43	48.1	47	116.4	0.22	0.09	0	5.6	0.76	25.3	243.5	1	116	54.9	70.9	0	242.8
*1*b	3	2	35.8	43.8	89.4	0.18	0.06	0	4.1	0.52	24.8	119.4	0	78	74	24	22	198
2	3	2.11	46.4	56.5	73	0.34	0.1	0	6.7	0.55	26.1	209.7	15	69.5	44.3	34	46.4	209.3
3	6	2.2	51.4	46.7	88.7	0.2	0.13	0	5.6	0.57	24.9	218.2	15.4	81.4	59.4	39.6	24.2	220

1=high-plateau profile; *1*b=forested slope profile; *2*=bare slope profile; *3*=low-plateau profile; n=number of samples; d=bulk density; Q=quartz; K=kaolinite; G=goethite; H=hematite; Gi=gibbsite.

TABLE 4

Bulk chemical and mineralogical average composition of the layers within the weathering profile of the high plateau expressed in gram per 100 cm^3 of sample

Depth (m)	n	d	SiO_2	Al_2O_3	Fe_2O_3	Mn_3O_4	MgO	K_2O	TiO_2	P_2O_5	H_2O	Total	Q	K	G	H	Gi	Total
9–8	2	2.65	27.8	36.3	161.6	0.1	0.1	0	4.9	2.4	32	265.2	5	87.5	156	10.6	0	259.1
6–4	2	2.47	39.5	41.2	136	0.25	0.1	0	5.6	0.77	24.7	248.1	0	100	60	87.5	0	247.5
3–4	1	2.35	65.3	58.7	77.3	0.16	0.07	0	5.6	0.75	26.4	243.3	2	148	44.6	37.6	0	232.2
3–0	5	2.75	40.4	50.6	146	0.2	0.05	0	5.8	1.1	27.7	271.8	3	85	52	104.5	30	274.5

n=number of samples; d=bulk density; Q=quartz; K=kaolinite; G=goethite; H=hematite; Gi=gibbsite.

TABLE 5

Bulk chemical and mineralogical average composition of massive (I) and nodular (II) iron duricrusts of each system expressed in gram per 100 cm^3 of sample

System	n	d	SiO_2	Al_2O_3	Fe_2O_3	Mn_3O_4	MgO	K_2O	TiO_2	P_2O_5	H_2O	Total	Q	K	G	H	Gi	Total
*1*a	5	2.75	40.4	50.6	146	0.2	0.05	0	5.8	1.1	27.7	271.8	3	85	52	104.5	30	274.5
*1*b	9	2.66	28.1	47.6	150.7	0.18	0.1	0	4.7	0.92	29.2	261.5	2.5	58	73.5	84	39.4	257.4
2	5	2.55	28.5	51.5	140.6	0.15	0.08	0	6.2	1.1	27.7	255.8	10	39	44	106	57	256
*3*a	5	2.45	38.7	47.2	127.2	0.15	0.05	0	3.7	0.71	26.7	244.4	7.3	71	46.5	88.2	31.8	244.8
*3*b	11	2.5	40.9	43.4	129	0.17	0.07	0	3.9	1.15	29.4	248	7.5	97.5	115	25	7.5	252.5

*1*a=high-plateau profile; *1*b=forested slope profile; *2*=bare slope profile; *3*a, *3*b=low-plateau profiles (*3a*=purple reddish nodular iron duricrust, *3*b=ochre brownish nodular or vermiform iron duricrust); n=number of samples; d=bulk density; Q=quartz; K=kaolinite; G=goethite; H=hematite; Gi=gibbsite.

lar duricrust slope. As illustrated in Fig. 6, the iron duricrusts are not well differentiated by their trace-element compositions either for transition elements or alkali-earth and rare-earth elements.

From the saprolite to the iron duricrust, the layers have a specific mineralogical signature pointing out the lateral and vertical evolution of saprolitization and ferruginization developments. In contrast, the trace-element signatures of the saprolite layers are not preserved in the upperlying layers at the scale of bulk samples, revealing the partial loss of the geochemical inheritance of the parent rock during increasing ferruginization processes. As this partial loss can result from averaging calculations, a complementary statistical study will give more detailed information about the relationships between elements and minerals during weathering.

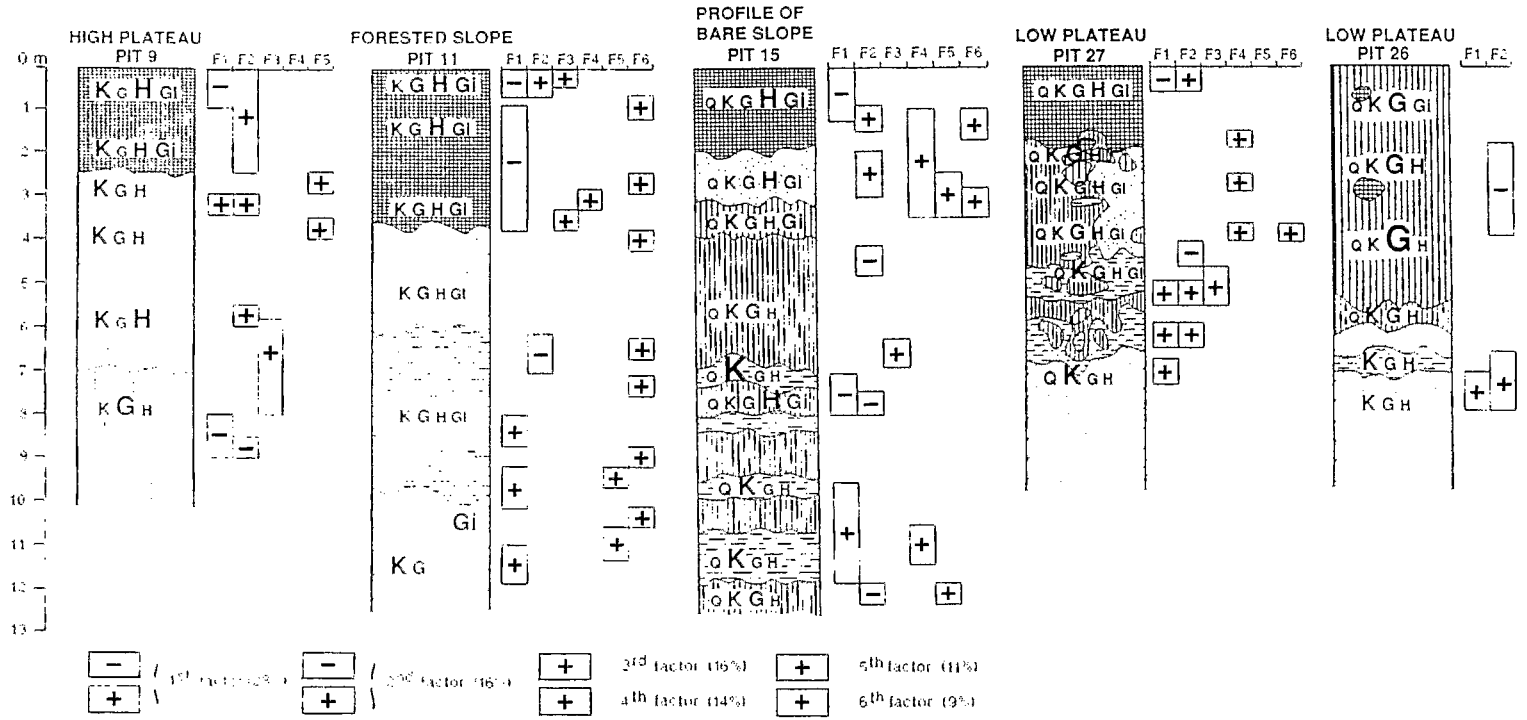

Fig. 7. Geochemical pathways of weathering profiles after Varimax rotated factor analysis (qualitative XRD results are given for each sample). *Q*=quartz; *K*=kaolinite; *G*=goethite; *H*=hematite; *Gi*=gibbsite; *very large letters*=very abundant; *large letters*=*abundant*; *letters*=fairly abundant; *small letters*=less abundant; *very small letters*=scarse).

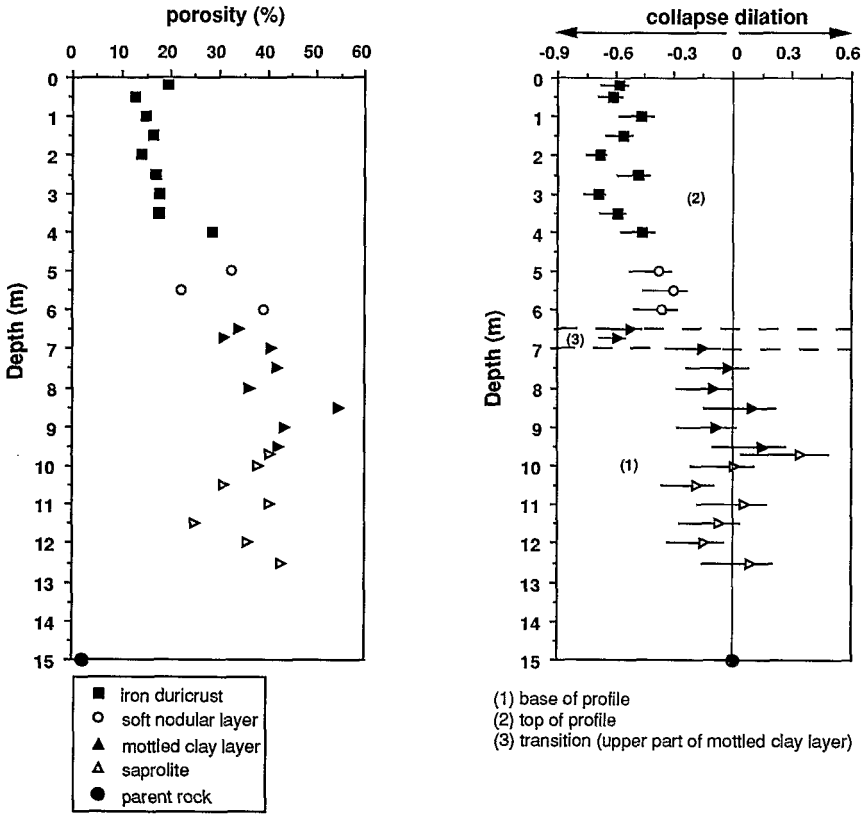

Fig. 8. Physical properties of a typical weathering profile (Pit *11*) as a function of depth.

5.2. Statistical relationships between minerals and chemical elements

Factor analysis has been carried out on mineralogical and chemical data (32 variables) for a whole of 100 samples collected within the weathering layers of each profile.

Varimax rotated factor analysis reveals 6 factors scores accounting for 94% of the total sample variance (Fig. 7). These factors highlight the opposite pathways between saprolitization and ferruginization processes.

The first factor opposes "hematite with Fe–V" (negative correlation) which pertains to ferruginization, and "kaolinite with Si–Al–Ti–Y–Yb" (positive correlation) which characterizes saprolitization (Fig. 7).

The second factor reveals the antagonism between hematite (positive correlation) and "goethite–P–Zn–Cu–Sc–Y" clustering (negative correlation), reflecting two ferruginization pathways. The first expressed the hematite-rich massive or nodular iron duricrusts and the second the goethite-rich nodular iron duricrust or indurated mottled clay layer development (Fig. 7).

The third factor groups together P, Ba, Sr, La and Ce (positive correlation), which manifests either the inheritance of monazite (Mazaltarim, 1989) or the supergene formation of gorcexite or florencite within the indurated mottled clay layers (Braun et al., 1990), or still the neoformation of cerianite at the lower part of the soft nodular layer in the high-plateau profile (Fig. 5-4 and -5).

The three former factors highlight a similar geochemical pathway between the base of the high-plateau profile, where an iron duricrust is forming, and the top of the forested slope profile where a nodular iron duricrust developed.

TABLE 6

Results of mass-transfer analysis applied on the pit *11*

Depth (m)	Type	ρ_w	ρ_g	Porosity (%)	ϵ	τ_{Si}	τ_{Al}	τ_{Fe}	τ_{Ti}	τ_{Mn}	τ_P	τ_V	τ_{Cr}
0.20	I	2.50	3.10	19.35	−0.58	−0.92	−0.53	0.57	−0.30	−0.81	−0.61	1.06	0.24
0.50	I	2.75	3.15	12.70	−0.61	−0.93	−0.61	0.72	−0.33	−0.88	−0.64	1.12	0.55
1.00	I	2.60	3.05	14.75	−0.47	−0.88	−0.38	0.98	−0.27	−0.85	−0.59	1.34	−0.20
1.50	I	2.70	3.23	16.41	−0.56	−0.91	−0.56	0.87	−0.34	−0.89	−0.58	1.30	0.21
2.00	I	2.80	3.25	13.85	−0.68	−0.94	−0.67	0.42	−0.51	−0.84	−0.63	0.59	0.23
2.50	I	2.55	3.07	16.94	−0.48	−0.89	−0.54	1.06	−0.34	−0.86	−0.50	1.35	0.10
3.00	I	2.65	3.22	17.70	−0.69	−0.95	−0.69	0.29	−0.52	−0.93	−0.59	0.29	−0.14
3.50	I	2.60	3.16	17.72	−0.59	−0.93	−0.63	0.71	−0.44	−0.85	−0.46	0.72	0.21
4.00	I	2.20	3.07	28.34	−0.46	−0.90	−0.53	0.77	−0.38	−0.87	−0.40	0.82	0.01
5.00	II	1.90	2.81	32.38	−0.38	−0.83	−0.42	0.30	−0.12	−0.81	−0.66	0.91	−0.37
5.50	II	2.10	2.70	22.22	−0.30	−0.81	−0.33	0.80	0.03	−0.79	−0.47	1.76	−0.24
6.00	II	1.80	2.96	39.19	−0.36	−0.88	−0.48	0.49	−0.04	−0.81	−0.70	1.24	0.06
6.50	IIIa	1.80	2.72	33.82	−0.52	−0.89	−0.57	−0.06	−0.08	−0.81	−0.69	0.03	−0.78
6.70	IIIa	1.90	2.75	30.91	−0.59	−0.91	−0.64	−0.08	−0.27	−0.83	−0.69	0.12	−0.54
7.00	IIIb	1.60	2.70	40.74	−0.15	−0.82	−0.22	0.26	0.23	−0.71	−0.70	0.95	−0.15
7.50	IIIb	1.57	2.70	41.85	−0.02	−0.78	−0.25	0.60	0.33	−0.70	−0.64	1.61	−0.28
8.00	IIIb	1.60	2.50	36.00	−0.10	−0.74	−0.22	0.20	0.28	−0.69	−0.75	0.87	−0.63
8.50	IIIb	1.18	2.60	54.62	0.10	−0.80	−0.31	0.22	0.51	−0.70	−0.71	0.92	−0.34
9.00	IIIb	1.34	2.37	43.46	−0.08	−0.80	−0.35	0.16	0.43	−0.73	−0.67	0.78	−0.42
9.50	IIIb	1.30	2.25	42.22	0.15	−0.70	−0.18	0.15	0.34	−0.73	−0.75	0.80	−0.40
9.70	IV	1.37	2.30	40.43	0.34	−0.90	0.56	0.28	0.60	−0.67	−0.50	0.96	−0.21
10.00	IV	1.36	2.19	37.90	0.01	−0.94	−0.01	0.35	0.74	−0.66	−0.39	1.11	−0.02
10.50	IV	1.60	2.32	31.03	−0.18	−0.75	−0.26	0.05	0.54	−0.60	−0.65	0.73	−0.35
11.00	IV	1.36	2.28	40.35	0.06	−0.78	−0.30	0.53	0.36	−0.59	−0.56	1.25	0.08
11.50	IV	1.70	2.26	24.78	−0.07	−0.66	−0.07	0.07	0.37	−0.52	−0.54	1.22	−0.28
12.00	IV	1.50	2.34	35.90	−0.14	−0.72	−0.28	−0.09	0.24	−0.70	−0.62	0.33	−0.42
12.50	IV	1.40	2.45	42.86	0.09	−0.71	−0.21	0.29	0.37	−0.62	−0.46	0.89	−0.12
15.00	parent rock	2.94	3.00	2.00	0.00	0.00	0.00	0.00	0.00	0.00	0.00	0.00	0.00

The fourth factor draws together quartz, Zr and Nb (positive correlation). Quartz as relict phase and zircon as weathering-resistant mineral characterizes the mineralogical inheritance of the parent rock, which is better marked in the slopes and the low-plateau profiles.

The fifth factor correlates Mn, Ba, Ni, Co and Zn (positive correlation), which are components of Mn-oxyhydroxides or asbolanes resulting from supergene precipitation within the weathering profiles under specific geochemical conditions (Parc et al., 1989). Lithiophorite was observed at the base of the high-plateau profile (Fig. 5-3, -4 and -5). However, this cluster does not discriminate the layers.

The sixth factor associates the gibbsite and alumina (positive correlation), reflecting the gibbsitization processes which substitutes for kaolinitization within the saprolite and iron duricrusts of the slope profiles.

5.3. Mass element transfers during saprolitization and ferruginization processes

Mass-balance calculations have been carried out from Pit 11 samples, in order to quantify net mass element transfers during weathering processes.

The bulk porosity globally increases from 2% in the parent rock to 40% at the base of the

τ_{Co}	τ_{Ni}	τ_{Cu}	τ_{Zn}	τ_{Sc}	τ_{Sr}	τ_{Y}	τ_{Nb}	τ_{Ba}	τ_{La}	τ_{Ce}	τ_{Yb}	τ_{Lu}
−0.89	−0.80	0.09	−0.73	−0.78	−0.72	−0.83	0.62	−0.60	1.98	0.65	−1.00	−1.00
−0.89	−0.78	0.33	−0.74	−0.73	−0.95	−0.88	0.88	−0.91	0.03	−0.08	−1.00	−1.00
−0.83	−0.76	1.38	−0.59	−0.57	−0.98	−0.83	1.29	−0.95	−0.14	−0.01	−1.00	−1.00
−0.92	−0.83	0.30	−0.71	−0.67	−0.97	−0.87	0.72	−0.92	−0.08	0.89	−1.00	−1.00
−0.91	−0.89	−0.18	−0.78	−0.77	−0.93	−0.88	1.22	−0.87	−0.22	−0.17	−1.00	−1.00
−0.82	−0.67	1.00	−0.65	−0.58	−0.93	−0.78	0.78	−0.86	1.01	0.51	−1.00	−1.00
−0.89	−0.85	−0.16	−0.83	−0.75	−0.97	−0.85	0.92	−0.94	−0.15	−0.25	−1.00	−1.00
−0.87	−0.83	0.38	−0.75	−0.68	−0.97	−0.85	1.39	−0.94	−0.28	−0.12	−1.00	−1.00
−0.90	−0.81	0.95	−0.70	−0.65	−0.98	−0.82	1.09	−0.98	−0.63	−0.13	−1.00	−1.00
−0.93	−0.80	1.14	−0.69	−0.68	−0.99	−0.76	1.65	−0.99	−0.82	−0.17	−0.67	−1.00
−0.85	−0.73	1.61	−0.54	−0.56	−0.99	−0.72	0.97	−0.99	−0.77	0.08	−0.79	−1.00
−0.95	−0.85	0.89	−0.59	−0.68	−0.99	−0.77	1.27	−0.99	−0.68	−0.14	−0.84	−0.21
−0.90	−0.86	0.60	−0.69	−0.71	−0.99	−0.80	1.69	−0.99	−0.38	−0.47	−0.63	−0.11
−0.96	−0.84	0.94	−0.73	−0.69	−0.99	−0.71	0.85	−0.99	−0.56	−0.60	−0.56	−0.20
−0.92	−0.78	0.63	−0.55	−0.55	−0.99	−0.71	1.09	−0.99	−0.54	0.10	−0.62	−0.31
−0.86	−0.68	1.40	−0.57	−0.49	−0.99	−0.63	1.53	−0.99	−0.62	0.47	−0.56	0.31
−0.90	−0.62	0.99	−0.57	−0.58	−0.99	−0.67	1.37	−0.99	−0.69	−0.12	−0.59	−0.02
−0.94	−0.74	0.83	−0.65	−0.58	−1.00	−0.74	1.27	−0.99	−0.72	−0.28	−0.82	0.10
−0.90	−0.67	0.66	−0.72	−0.60	−1.00	−0.69	1.17	−0.99	−0.62	−0.17	−0.65	−0.37
−0.89	−0.54	0.46	−0.54	−0.58	−1.00	−0.59	1.16	−0.99	−0.72	−0.38	−0.79	0.02
−0.93	−0.63	0.53	−0.34	−0.55	−0.99	−0.72	1.09	−0.98	0.14	−0.13	−0.74	−1.00
−0.92	−0.83	−0.03	−0.76	−0.52	−1.00	−0.86	1.12	−0.98	−0.87	1.75	−1.00	−0.53
−0.80	−0.48	0.18	−0.63	−0.53	−1.00	−0.74	0.89	−0.98	−0.84	−0.18	−0.63	−1.00
−0.81	−0.46	−0.11	−0.60	−0.45	−1.00	−0.76	0.19	−0.95	−0.87	0.20	−0.80	−0.27
−0.73	−0.41	0.45	−0.29	−0.38	−1.00	−0.68	0.47	−0.91	−0.75	1.18	−0.78	−1.00
−0.95	−0.70	0.27	−0.61	−0.56	−1.00	−0.53	0.86	−0.97	−0.80	0.25	−0.09	−0.12
−0.94	−0.46	0.94	−0.66	−0.43	−1.00	−0.75	0.88	−0.97	−0.86	−0.22	−0.89	−1.00
0.00	0.00	0.00	0.00	0.00	0.00	0.00	0.00	0.00	0.00	0.00	0.00	0.00

I = iron duricrust; II = soft nodular layer; III = mottled clay layer (a = upper part, b = lower part); IV = saprolite; ρ_w = bulk density; ρ_g = grain density; ϵ = volume change (− = collapse, + = dilation); τ = mass transport factor (+ = gain, − = loss); Ca, Mg, Na, K and Eu are not taken in account because they are entirely leached ($\tau = -1$).

mottled clay layer, and then decreases progressively toward the surface to reach ~15% within the iron duricrust layer (Fig. 8).

Volumetric changes calculated with Zr as immobile element well differentiate two parts within the profile (Fig. 8):

(1) The base, that is the parent rock, the saprolite and the lower part of the mottled clay layer where the weathering is isovolumetric except for the dilational gibbsite-richest saprolite.

(2) The top, that is the upper part of the mottled clay layer, the soft nodular layer and the iron duricrust where the weathering is collapse-controlled with a volumetric change ranging from −0.68 to −0.3. The transition between the two parts (upper part of mottled clay layer noted 3 in Fig. 8) is strongly marked, compared to the isovolumetric saprolite, by a collapse of 55% with respect to the parent rock.

Results of mass-transport function calculations are reported in Table 6, and allow us to differentiate three groups of elements from their behaviour within the whole weathering profile:

— Group 1: Fe, V, Cu and Nb: all these elements are imported during weathering processes from external sources. The amount of imported Fe increases clearly toward the surface.

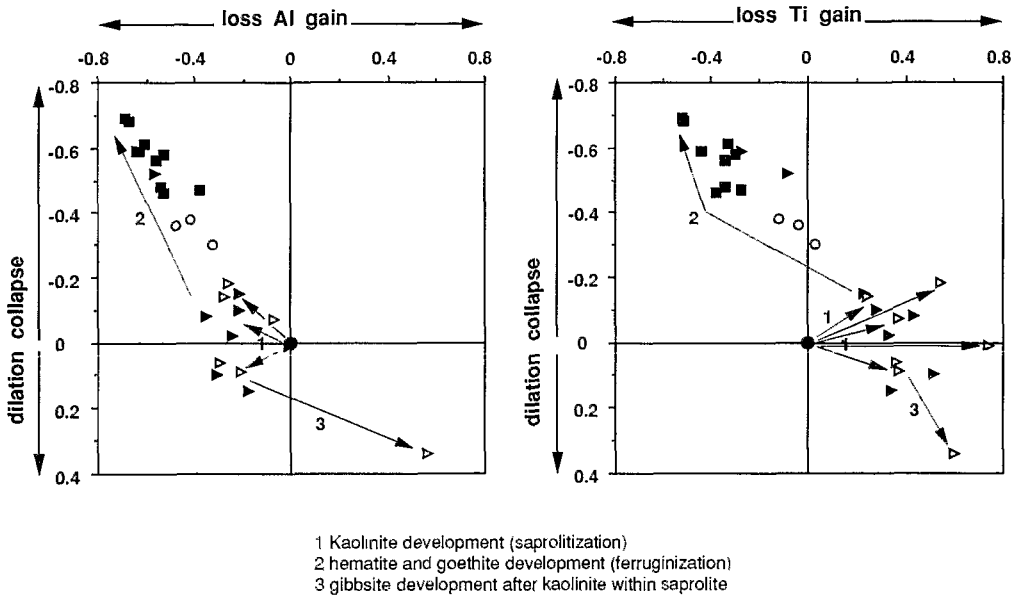

Fig. 9. Comparison of mass-transport factor of Al and Ti as a function of volume change.

— Group 2: Si, Mn, Co, Ni, Zn, Sc, Sr, Y, Ba, Yb and Lu: these elements are stronghly leached out of the global weathering system, with a higher rate in the soft nodular and iron duricrust layers than in the mottled clay layer and saprolite.

— Group 3: Al, Ti, P, Cr, La and Ce: these elements have a global irregular behaviour in terms of gains and losses, which can only be explained by local environmental conditions at the scale of the weathering layers. For example, a net gain in Ce is recorded in the saprolite, due to downward Ce solute translocation from the nodular layer and the base of the iron duricrust (depletive values of the transport function), leading to cerianite formation within the saprolite, as it was already observed in a similar weathering system (Braun et al., 1990). At the top of the weathering system, the nodular iron duricrust is Ce-enriched compared to the parent rock. This geochemical behaviour of Ce corroborates the petrological and the statistical analysis investigations which had respectively shown: (1) the preciptitation of cerianite in a forming iron duricrust at the base of the high-plateau profile; and (2) the geochemical relationship between the latter and the nodular iron duricrust of the forested slope profile.

Some of these elements, such as Al and Ti, are good pathfinders to trace saprolitization and ferruginization processes. This is shown by representing the weathering pathways as functions of volumetric changes and Al or Ti net mass transfers (Fig. 9).

As saprolite differentiates from fresh parent rock, and into basal mottled clay layer, Al is weakly leached out during quite isovolumetric changes: this is the domain where kaolinite develops with a gain in Ti, i.e. the saprolitization domain. Gibbsite formation is obviously characterized by a net gain in Al and Ti, and a positive volumetric change (Fig. 9).

From the upper part of the mottled clay layer to the iron duricrust, the amount of both leached Al and Ti increases as well as collapses. This is the domain of goethite and hematite formation, i.e. the ferruginization domain.

Quantification of the overall mass transfer during both saprolitization and ferruginization processes can be approached by estimat-

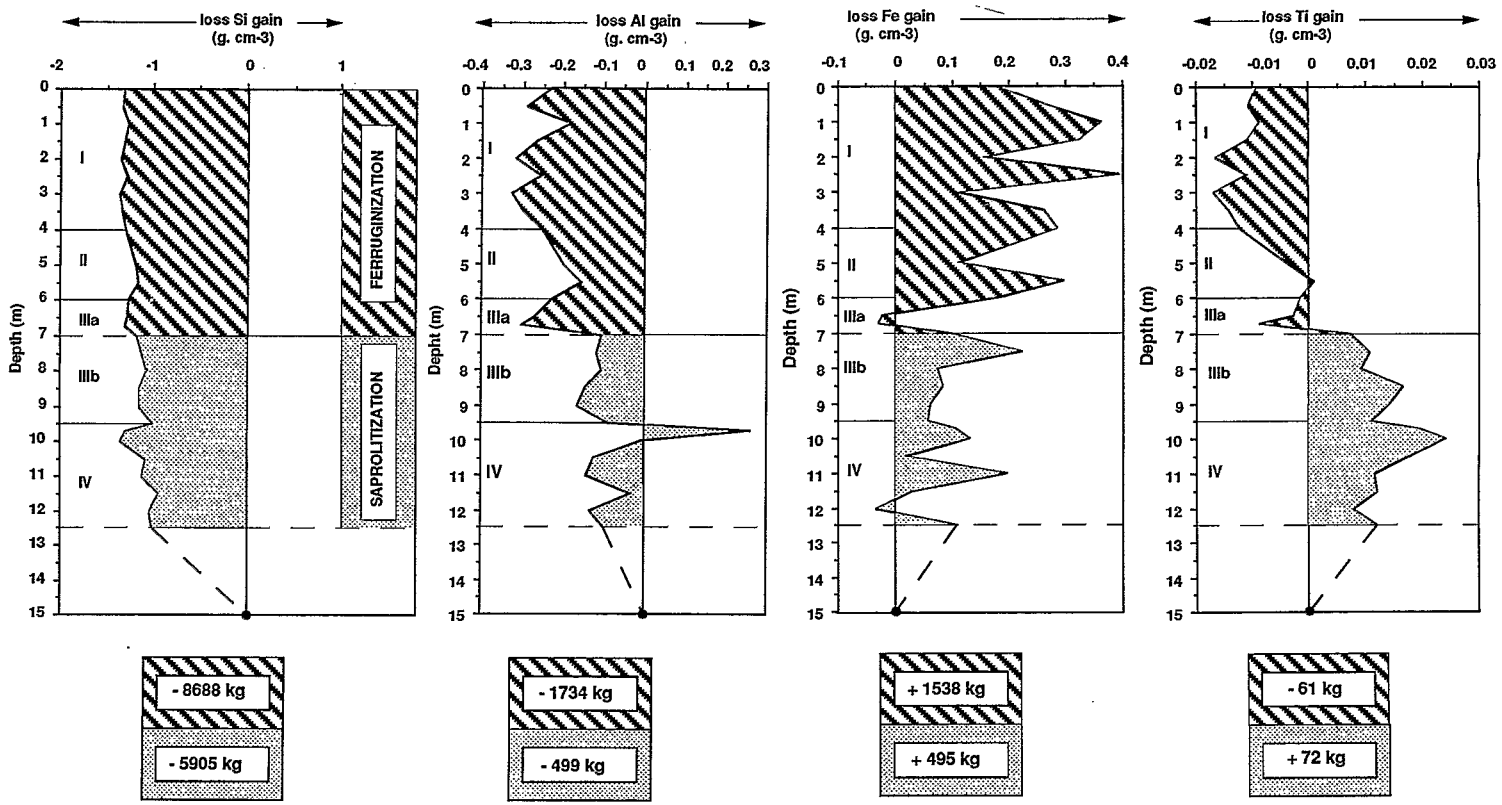

Fig. 10. Comparison of the total mass transfer of Si, Al, Fe and Ti as a function of depth and of both saprolitization and ferruginization processes.

ing the transfers of the main chemical components which are Si, Al, Fe and Ti.

The total mass of any mobile element j transferred through a weathering system w can be calculated from:

$$m_{j,w} = \left(\frac{C_{j,p}}{100}\rho_p v_p\right)\tau_{j,w} \quad (4)$$

This equation gives the transferred mass for a single volume V_p. To calculate the total mass transferred through a weathering system (defined by a cross-sectional area, and expressed in kilograms) to an investigated depth Z_n, it is necessary to integrate the $t_{j,w}$ as a function of depth:

$$M_{j,w} = \left(\frac{C_{j,p}}{100}\rho_p\right)\int_{z=0}^{z=z} {}^{n}\tau_{j,w}\,dz \quad (5)$$

Results are graphically representated in Fig. 10. The net mass transfers of Si, Al, Fe and Ti are a function of both saprolitization and ferruginization processes. The saprolitization development for 5.5-m thickness corresponds to a leaching of 5905 kg Si and 499 kg Al, and to an accumulation of 495 kg Fe and 72 kg Ti. The development of 7 m of ferruginous profile including the upper part of the mottled clay layer, the soft nodular layer and the iron duricrust, involves net losses of 8688 kg Si, 1734 kg Al and 61 kg Ti on the one hand, and a net gain of 1538 kg Fe, on the other. The mass-balance transfer of Ti is globally positive (+11 kg) according to anatase precipitation within the fine porosity structure crossing the saprolite.

6. Discussion and conclusions

The three iron duricrust systems have been distinguished by their geomorphological outlines as well as by the petrographical, petrological and geochemical features of the constituent layers.

Geochemical differentiation of the saprolites reflects either the variety of parent rocks (Leprun, 1979; Pion, 1979; Ambrosi and Nahon, 1986, Nahon, 1986) or the variation in morpho-pedological paths (Bocquier, 1971; Boulet, 1974; Nahon, 1976; Boulet et al., 1977; Bocquier et al., 1983). In fact, from a similar parent rock and under similar climatic conditions, both saprolitization and ferruginization processes are more advanced on the highest and best drained parts of the landscape than on the lowest parts. In addition, erosion is stronger on the slopes and low plateaus near the thalwegs (Grandin, 1973), leading to the rejuvenation of weathering layers, and sometimes favouring their outcropping (Tardy et al., 1988c; Mazaltarim, 1989). In this case, the saprolite of the low-plateau profile is younger and less mature than the saprolite of the forested slope profile.

Secondary ferruginization processes involve the development of successive layers from the bottom to the top of profiles for each system such as mottled clay layer, indurated mottled clay layer, soft nodular layer and iron duricrust. These layers are subjected to hematitization and goethitization processes which take place with morpho-pedoclimatic changes.

Within the soft nodular layer, two populations of nodules with various origins have been studied. The lithomorphous nodules result from ferruginization of saprolite domains, whereas the argillomorphous nodules originate from the ferruginization of mottled clay layer domains.

In the case of saprolite, primary ferruginization is goethitic and derives from weathering of Fe-bearing primary minerals and it becomes progressively hematitic within the mottled clay layer and within the soft nodular layer during oxidation processes. In the latest stage, goethite develops as cortex or a brown network around or within hematitic nodules.

Goethite formation affects the iron duricrusts as well as nodules of the soft nodular layers or the indurated mottled clay layers. In this way, goethite content increases at the expense of hematite. This mineralogical trans-

formation can be accompanied by gibbsite crystallization in the nodules. Gibbsite derived either from in situ kaolinite hydrolysis or from inheritance of past more humid climatic conditions, according to its occurrence in the nodular iron duricrust of the slope profiles. The nodules of the soft nodular layer, containing inherited gibbsite crystallites may result from the geochemical degradation of a former gibbsite-rich nodular iron duricrust. This interpretation is confirmed by the occurrence of an Fe-depleted clayey layer in the upper part of the soft nodular layer, and by the presence of an Fe-enriched layer at the base of the soft nodular layer in the high-plateau profile.

As previously demonstrated, the equilibrium reactions between hematite and goethite, and between kaolinite and gibbsite are controlled by changes in temperature, pore size, water and silica activities and also oxygen and carbon dioxide fugacities (Didier et al., 1985; Tardy and Nahon, 1985; Trolard and Tardy, 1987; Tardy and Novikoff, 1988; Tardy et al., 1988b; Ambrosi, 1990). These physico-chemical parameters characterize the pedo-bioclimatic environment of mineral formation.

Hematite and kaolinite are tightly associated within the iron duricrusts of the high-plateau profiles, where the clayey material porosity is fine ($< 10\,\mu m$) and the water activity is less than 1. Such a mineralogical association gives way to goethite and gibbsite wherever porosity, water activity and carbon dioxide fugacity increase and in the same time silica activity and oxygen fugacity decrease. This is the case within the high-plateau and the forested slope profiles. The transformation of the kaolinite into gibbsite through halloysite is efficient in the saprolite layer of the forested slope profile, according to the physico-chemical features changes of the microenvironment (Trolard et al., 1990). The transformation of hematite into goethite under more humid conditions is observed within the indurated mottled clay layer in the high-plateau profile. Moreover, the coprecipitation of lithiophorite and cerianite (Fig. 5-3, -4 and -5) in this layer indicates oxidizing conditions, leading to the development of a recent iron duricrust. This mineral assemblage is in good agreement with the thermodynamic stability of lithiophorite (Parc, 1989) and cerianite (Braun et al., 1990).

The massive and nodular iron duricrusts are sequentially formed in space and time under the effect of Fe-aggradation and -degradation processes. In fact, the hematite-rich massive iron duricrust of the high plateau results from Fe-aggradation processes, whereas the nodular iron duricrust of the slope generate from Fe-degradation processes. In contrast, the goethite-rich indurated mottled clay layers result from both Fe-aggradation and -degradation processes in more humid and less oxidizing conditions.

Thus, the formation and transformation of the iron duricrust systems are functions of discriminating saprolitization and ferruginization processes. Both lead to aggraded and degraded ferrruginous layer formation in agreement with morpho-pedoclimatic changes. Stability of minerals varies from the upper parts of the landscape to the lower ones, or from the top to the base of weathering profiles. Therefore, goethite-rich layers succeed to hematitic-rich ones. Kaolinite is the dominant clay in the unattacked layers but it transforms into gibbsite under more humid and better drainage conditions.

The Varimax rotated factor analysis shows that the relationships between the secondary minerals and the trace elements are a function of saprolitization and ferruginization process intensity.

The saprolite of the low-plateau profile is rich in alkali earths (Sr, Ba), rare-earth elements (La, Ce) and also Y and Zr contents. The saprolite of the forested slope profile is more mature because it is the richest in Fe and particularly in goethite with higher contents of transition elements such as Mn, V, Ni, Co, Cr, Zn and Cu. Manceau and Calas (1986), Cor-

nell and Giovanoli (1987), Nunez and Gilkes (1987), Cornell (1988), and Schwertmann et al. (1989) demonstrated that transition elements substitute in tetrahedral or octahedral sites of Fe-oxyhydroxides or clays.

In addition to the fact that Ti, Zr and Nb are the main components of the residual mineral phases, the geochemical signature of parent rocks attenuates with increased ferruginization processes. Saprolitization process partially preserves the geochemical inheritance of parent rocks, whereas ferruginization process depletes it.

Mass-transfer analysis points out the geochemical systematics of a typical weathering system. It shows that the volume change (collapse and dilation) and the respective behaviours of Al and Ti accurrately emphasize the saprolitization and ferruginization pathways.

During the ferruginization process, transition elements segregate between hematite and goethite. The behaviour of Mn, Ni, Co, Zn, Sc and Cu is controlled by goethite development, whereas V and Cr behave like Fe with a weak affinity for hematite. Nevertheless, V and Cu are the only trace elements imported during weathering processes. The alkali earths and rare-earth elements also segregate during ferruginization. Ba and Ce are commonly linked to Mn-oxyhydroxides (Fortin, 1989; Braun et al., 1990) which can precipitate in ferruginous layers under moderate oxidizing conditions, whereas Sr, La, Eu, Yb and Lu are generally strongly released into solution. In our report, La accumulates in iron crust, while Ce behaves irregularly during the weathering processes, being either weakly leached or concentrated at the upper part of the weathering system (iron duricrust), or much strongly accumulated at the lower part (saprolite). The Ce enrichment can be explained by downward translocation during regolith reduction which has taken place during conversion of massive iron duricrust (similar to the existing high-plateau massive iron duricrust) into nodular iron duricrust most developed on the slopes.

Apart from the behaviour of trace elements, the mass-transfer analysis shows, during ferruginization development, the exportation of major elements such as Si, Al and Ti. Goethite and hematite are little Al-substituted, according to crystallochemical study coupled with microprobe analysis (Beauvais, 1991). Within saprolite, Fe and Ti are correlated because they accumulate with respect: (1) to relict unweathered ilmenite; (2) to geochemical vertical transport; and (3) to precipitation of anatase. In the same way, saprolite may be locally enriched with Al as a result of both kaolinization and vertical transport.

The behaviour of Al and Ti as well as the volume change accurately track the saprolitization and ferruginization processes (Figs. 8–10).

The study of chemical element behaviour in lateritic environment, either major elements (Al, Ti, etc.) or trace elements (Ce, etc.), is thus very efficient for a better understanding of the lateritic weathering system evolution. Furthermore, it shows that the trace element-bearing secondary minerals reflect the pedoclimatic conditions of their formation, and therefore, better the global climatic changes than some geochemical relationships with the parent rock. Thus, it enables us to propose a likely pattern of lateritic landscape development.

It is generally believed that the global lateritic systems formed from the West African shield derive from ancient massive bauxitic formations (Grandin, 1973; Boulangé, 1983; Boulangé and Millot, 1988). By contrast, our petrological and geochemical investigations show that the actual goethite- and gibbsite-rich lateritic systems mostly derive from previous hematite- and kaolinite-rich iron duricrusts similar to those still present on the high plateaus, rather than from an ancient bauxitic system. Although some light vestiges of pisolitic bauxite were discovered in the northern R.C.A. (Boulvert, 1990), this study found neither physical nor chemical evidence for the ex-

istence of such structures in the southern part of Central Africa.

However, this proposition implicates that a more tropical contrasted climate promoting the hematite-rich system prevailed before the present tropical humid episode, which is more favourable to goethite and gibbsite development. This conclusion is in good agreement with recent paleoclimatic reconstructions based on the mineralogical facies distribution of lateritic formations in Africa and Brazil (Tardy et al., 1988a, b, 1991; Beauvais, 1991).

Acknowledgements

This work was carried out thanks to the financial support of the research program PIRAT from INSU and ORSTOM. We are very grateful to the "Secrétariat à la Recherche Scientifique et Technique auprès de la Présidence de la République Centrafricaine". The authors are particularly indebted to Dr. D. Mazaltarim, Dr. J.C. Muller, Professor H. Paquet and Dr. C. Roquin ("Centre de Géochimie de la Surface" of Strasbourg) for mineralogical and chemical analysis support, and also to Ph. Karcher for his technical help during SEM observations. We are also grateful to B. Boulangé for helpful suggestions and critical review of the text. Our thanks are also due to R. Dassule and J.J. Motte for drafting the artwork.

References

Ambrosi, J.P., 1984. Pétrologie et géochimie d'une séquence de profils latéritiques cuirassés ferrugineux de la région de Diouga, Burkina Faso. Thèse 3è cycle, Univ. Poitiers, Poitiers, 223 pp.

Ambrosi, J.P., 1990. Modélisation thermodynamique de l'altération latéritique dans le système Fe_2O_3–Al_2O_3–SiO_2–H_2O. Ph.D. Thesis, University of Poitiers, Poitiers, 379 pp.

Ambrosi, J.P. and Nahon, D., 1986. Petrological and geochemical differentiation of lateritic iron crust profiles. Chem. Geol., 57: 371–393.

Beauvais, A., 1989. Étude pétrographique et géochimique de profils d'altération latéritique cuirassés dans le Sud-Est de la République Centrafricaine. Géodynamique, 4(2): 71–91.

Beauvais, A., 1991. Paléoclimats et dynamique d'un paysage cuirassé du Centrafrique — Morphologie, pétrologie et géochimie. Ph.D. Thesis, University of Poitiers, Poitiers, 317 p.

Beauvais, A. and Mazaltarim, D., 1988. Étude des cuirasses latéritiques dans la région de Dembia–Zémio en Centrafrique — Pétrographie, minéralogie et géochimie. Sci. Géol., Bull., Strasbourg, 44(1): 47–69.

Bocquier, G., 1971. Genèse et évolution de deux toposéquences de sols tropicaux du Tchad — Interprétation biogéodynamique. Thèse Sci., Univ. Strasbourg, Strasbourg and Mém. ORSTOM (Off. Rech. Sci. Tech. Outre-mer), Paris, 62(1973), 350 pp.

Bocquier, G., Boulangé, B., Ildefonse, P., Nahon, D. and Muller, D., 1983. Transfers, accumulation modes, mineralogical transformation and complexity of historical in lateritic profiles. In: A.J. Melfi and A. Carvahlo (Editors), Proc. 2nd Int. Symp. on Laterisation Processes, São Paulo, pp. 331–343.

Boski, T. and Herbosch, A., 1990. Trace elements and their relation to the mineral phases in the lateritic bauxites from southeast Guinea Bissau. Chem. Geol., 82: 279–297.

Boulangé, B., 1983. Les formations bauxitiques latéritiques de Côte d'Ivoire — Les faciès, leur transformation, leur distribution et l'évolution du modelé. Trav. Doc. ORSTOM (Off. Rech. Sci. Tech. Outre-mer), Paris, 175, 272 pp.

Boulangé, B. and Millot, G., 1988. La distribution des bauxites sur le craton ouest-africain. Sci. Géol., Bull., 41(1): 113–123.

Boulet, R., 1974. Toposéquences de sols tropicaux en Haute-Volta — Équilibres dynamiques et bioclimats. Thèse Sci., Univ. Strasbourg, Strasbourg, and Mém. ORSTOM (Off. Rech. Sci. Tech. Outre-mer), Paris, 85(1978), 272 pp.

Boulet, R., Bocquier, G. and Millot, G., 1977. Déséquilibre pédobioclimatique dans les couvertures pédologiques de l'Afrique tropicale de l'Ouest et son rôle dans l'aplanissement des reliefs. Sci. Géol., Bull., 30(4): 235–244.

Boulvert, Y., 1976. Types de modelés cuirassés. Intérêt morphopédologique des "lakérés" — Finesse, précision de la télédétection avec le couvert végétal (région de Dembia). Rev. Photo Interprét., 4: 18–29.

Boulvert, Y., 1983. Notice explicative de la carte pédologique de la République Centrafricaine à 1: 1 000 000. ORSTOM (Off. Rech. Sci. Tech. Outre-mer), Paris, 100, 126 pp.

Boulvert, Y., 1990. Contribution à l'étude du milieu naturel centrafricain — Exploitation et corrélation des données obtenues par photo-interprétation, télédétection et travaux de terrain, pour la réalisation des cartes pédologiques, phytogéographiques et géomorpholo-

giques à 1/1 000 000. de la République Centrafricaine. Thèse, Univ. Dijon. Dijon, 2 vols., 430 pp. (mimeographed).

Braun, J.J., Pagel, M., Muller, J.P., Bilong, P., Michard, A. and Guillet, B., 1990. Cerium anomalies in lateritic profiles. Geochim. Cosmochim. Acta, 54: 781–795.

Brimhall, G.H., Lewis, C.J., Ague, J.J., Dietrich, W.E., Hampel, J., Teague, T. and Rix, P., 1988. Metal enrichment in bauxites by deposition of chemically mature aeolian dust. Nature (London), 333: 819–824.

Butt, C.R.M., 1987. A basis for geochemical exploration models for tropical terrains. In: Y. Ogura (Guest-Editor). Proceedings of an International Seminar on Laterite, October 14–17, 1985, Tokyo, Japan. Chem. Geol., 60: 5–16 (special issue).

Colin, F. and Vieillard, P., 1991. Behavior of gold in lateritic equatorial environment: weathering and surface dispersion of gold residual particles at Dondo Mobi, Gabon. Appl. Geochem., 3: 279–290.

Colin, F., Lecomte, P. and Boulangé, B., 1989. Dissolution features of gold particles in a lateritic profile at Dondo Mobi, Gabon. Geoderma, 45: 241–250.

Colin, F.G., Brimhall, G.H., Nahon, D.B., Lewis, C.J., Baronnet, A. and Danty, K., 1992. Equatorial rainforest lateritic mantles: a geomembrane filter. Geology, 20: 523–526.

Cornell, R.M., 1988. The influence of some divalent cations on the transformation of ferrihydrite into more crystalline products. Clay Miner., 23: 329–332.

Cornell, R.M. and Giovanoli, R., 1987. Effect of manganese on the transformation of ferrihydrite to more crystalline products. Clays Clay Miner., 35(1): 11–20.

Davies, T.C. and Bloxham, T.W., 1979. Heavy metal distribution in laterites, southwest of regent, Freetown igneous complex, Sierra Leone. Econ. Geol., 74(3): 638–644.

De Carlo, E.H. and McMurtry, G.M., 1992. Rare-earth element geochemistry of ferromanganese crusts from the Hawaiian Archipelago, central Pacific. Chem. Geol., 95: 235–250.

Didier, Ph., Perret, D., Tardy, Y. and Nahon, D., 1985. Équilibres entre kaolinite ferrifères, goethites alumineuses et hématites alumineuses dans les systèmes cuirassés — Rôle de l'activité de l'eau et de la taille des pores. Sci. Géol., Bull., 38(4): 383–397.

Donkin, M.J. and Fey, M.V., 1991. Factor analysis of familiar properties of some Natal soils with potential for afforestation. Geoderma, 48(3-4): 297–304.

Freyssinet, Ph., Zeegers, H. and Tardy, Y., 1989. Morphology and geochemistry of gold grains in lateritic profile from South Mali. J. Geochem. Explor., 32: 99–116.

Grandin, G., 1973. Aplanissements cuirassés et enrichissement des gisements de manganèse dans quelques régions d'Afrique de l'Ouest. Thèse Sci., Univ. Strasbourg, Strasbourg, and Mém. ORSTOM (Off. Rech. Sci. Tech. Outre-mer), Paris, 82(1976), 275 pp.

Herbillon, A.J. and Nahon, D.B., 1988. Laterites and lateritization processes. In: J.W. Stucki, B.A. Goodman and U. Schwertmann (Editors), Iron in Soils and Clay Minerals. N.A.T.O. (N. Atlantic Treaty Org.), ASI (Adv. Stud. Inst.), Ser. C, 217: 779–796.

Jöreskog, K.G., Klovan, J.E. and Reyment, R.A., 1976. Geological Factor Analysis. Elsevier, Amsterdam.

Lebart, L., Morineau, A. and Fenelon, J.P., 1979. Traitement des données statistiques. Dunod, Paris, 510 pp.

Lecomte, P. and Colin, F., 1989. Gold dispersion in a tropical rainforest weathering profile at Dondo Mobi, Gabon. J. Geochem. Explor., 34: 285–301.

Leprun, J.C., 1979. Les cuirasses ferrugineuses des pays cristallins de l'Afrique occidentale sèche — Genèse, Transformation, Dégradation. Mém. Sci. Géol., Strasbourg, 58: 224 pp.

Litaor, M.I., Dan, Y. and Koyumdjisky, H., 1989. Factor analysis of a lithosequence in the northeastern Samaria steppe (Israel). Geoderma, 44: 1–15.

Lucas, Y., 1989. Systèmes pédologiques en Amazonie brésilienne — Équilibres, déséquilibres et transformations. Thèse Doct., Univ. Poitiers, Poitiers, 157 pp.

Maignien, R., 1958. Le cuirassement des sols en Guinée. Mém. Serv. Carte Géol. Alsace–Lorraine, Strasbourg, 16, 204 pp.

Manceau, A. and Calas, G., 1986. Nickel-bearing clay minerals, 2. Intracrystalline distribution of nickel: a X-ray absorption study. Clay Miner., 21(3): 341–360.

Martin, D., 1966. Études pédologiques dans le Centre Cameroun, Nanga–Eboko à Bertoua. Mém. ORSTOM (Off. Rech. Sci. Tech. Outre-mer), Paris, 19, 92 pp.

Martin, D., Chatelin, Y., Collinet, J., Guichard, E. and Sala, G., 1981. Les sols du Gabon — Pédogenèse, répartition et aptitudes — Notice explicative de la carte pédologique à 1: 200 000. ORSTOM (Off. Rech. Sci. Tech. Outre-mer), Paris, 92, 65 pp.

Matheis, G., 1981. Trace element patterns in lateritic soils applied to geochemical exploration. J. Geochem. Explor., 15(1-3): 471–480.

Mazaltarim, D., 1989. Géochimie des cuirasses ferrugineuses et bauxitiques de l'Afrique de l'Ouest et Centrale. Thèse Doct., Univ. Strasbourg, Strasbourg, 260 pp.

McFarlane, M.J., 1976. Laterites and Landscapes. Academic Press, London, 151 pp.

Mestraud, J.P., 1982. Géologie et ressources minérales de la République Centrafricaine — État des connaissances fin 1963. Mém. B.R.G.M. (Bur. Rech. Géol. Min.), Orléans, 60, 185 pp.

Muller, D., Boucquier, G., Nahon, D. and Paquet, H., 1981. Analyses des différenciations minéralogiques et structurales d'un sol ferrallitique à horizons nodulaires du Congo. Cah. ORSTOM (Off. Rech. Sci. Tech. Outre-mer), Sér., Pédol., 18(2): 87–109.

Muller, J.P., 1987. Analyse pétrologique d'une formation latéritique meuble du Cameroun — Essai de traçage d'une différenciation supergène par les paragenèses minérales secondaires. Thèse Sci., Univ., Paris VI, Paris, 188 pp.

Muller, J.P. and Bocquier, G., 1986. Dissolution of kaolinites and accumulation of iron oxides in lateritic–ferruginous nodules — Mineralogical and microstructural transformations. Geoderma, 37: 113–136.

Munsell®, 1954. Munsell Soil Colour Charts. Munsell Color Co., Baltimore, Md.

Nahon, D., 1976. Cuirasses ferrugineuses et encroûtements calcaires au Sénégal occidental et en Mauritanie — Systèmes évolutifs: géochimie, structures, relais et coexistence. Thése Sci., Univ. Aix-Marseille III, Marseille, and Mém. Sci. Géol., Strasbourg, 44(1976), 232 pp.

Nahon, D.B., 1986. Evolution of iron crusts in tropical landscapes. In: S.M. Colman and D.P. Dethier (Editors), Rates of Chemical Weathering of Rocks and Minerals. Academic Press, London, pp. 169–187.

Novikoff, A., 1974. L'altération des roches dans le Massif du Chaillu (République du Congo) — Formation et évolution des argiles en zone ferrallitique. Thèse Sci., Univ. Strasbourg, Strasbourg, 298 pp.

Nunez, R.L. and Gilkes, R.J., 1987. Acid dissolution of synthetic metal-containing goethites and hematites. In: L.C. Schultz, H. Van Olphen and F.A. Mumpton (Editors), Proc. Int. Clay Conf., Denver, 1985. Clay Miner. Soc., Bloomington, Ind., pp. 197–204.

Parc, S., 1989. Contribution à l'étude cristallochimique et thermodynamique des oxyhydroxydes de manganèse dans l'altération latéritique. Thèse Doct., Univ. Aix-Marseille III, Marseille, 129 pp.

Parc, S., Nahon, D., Tardy, Y. and Vieillard, Ph., 1989. Estimated solubility products and fields of stability for cryptomelane, nsutite, birnessite and lithiophorite based on natural lateritic weathering sequences. Am. Mineral., 74: 466–475.

Pion, J.C., 1979. Altération des massifs cristallins basiques en zone tropicale sèche — Étude de toposéquences en Haute-Volta. Mém. Sci. Géol., Strasbourg, 57, 220 pp.

Poidevin, J.L., 1991. Les ceintures de roches vertes de la Républiques Centrafricaine (Bandas, Boufoyo, Bogoin et Mbomou) — Contribution à la connaissance du Précambrien du Nord du craton du Congo. Thèse Doct. Sci., Univ. Clermont-Ferrand II, Clermont-Ferrand, 440 pp.

Roquin, C., Freyssinet, Ph., Zeegers, H. and Tardy, Y., 1990. Element distribution patterns in laterites of southern Mali: consequence for geochemical prospecting and mineral exploration. Appl. Geochem., 5: 303–315.

SAS (Statistical Analysis System), 1985. User's Guide: Statistics, Version 5 edition. SAS Inst. Inc., Cary, N.C., 956 pp.

Schwertmann, U., Gasser, U. and Sticher, H., 1989. Chromium for iron substitution in synthetic goethites. Geochim. Cosmochim. Acta, 53(6): 1293–1297.

Tardy, Y. and Nahon, D., 1985. Geochemistry of laterites, stability of Al-goethite, Al-hematite, and Fe^{3+}-kaolinite in bauxites and ferricretes — An approach to the mechanism of concretion formation. Am. J. Sci., 285: 865–903.

Tardy, Y. and Novikoff, A., 1988. Activité de l'eau et déplacement des équilibres gibbsite–kaolinite dans les profils latéritiques. C.R. Acad. Sci., Paris, Sér. II, 306: 39–44.

Tardy, Y., Melfi, A.J. and Valeton, I., 1988a. Climats et paleoclimats tropicaux periatlantiques — Rôle des facteurs climatiques et thermodynamiques: température et activité de l'eau sur la répartition et la composition minéralogique des bauxites et des cuirasses ferrugineuses, au Brésil et en Afrique. C.R. Acad. Sci., Paris, Sér. II, 306: 289–295.

Tardy, Y., Bardossy, G. and Nahon, D., 1988b. Fluctuations de l'activité de l'eau et successions des minéraux hydratés et déshydratés au sein de profils latéritiques ferrugineux et bauxitiques. C.R. Acad. Sci., Paris, Sér. II, 307: 753–759.

Tardy, Y., Kobilsek, B., Roquin, C. and Paquet, H., 1990. Influence of periatlantic climates and paleoclimates on the distribution and mineralogical composition of bauxites and ferricretes. In: Y. Noack and D. Nahon (Editors), Geochemistry of the Earth's Surface and of Mineral Formation. Chem. Geol., 84: 179–182 (special issue; extended abstract).

Tardy, Y., Kobilsek, B. and Paquet, H., 1991. Mineralogical composition and geographical distribution of African and Brazilian periatlantic laterites — The influence of continental drift and tropical paleoclimates during the past 150 million years and implications for India and Australia. J. Afr. Earth Sci., 12(1/2): 283–295.

Trolard, F. and Tardy, Y., 1987. The stabilities of gibbsite, boehmite, aluminous goethites and aluminous hematites in bauxites, ferricretes and laterites as a function of water activity, temperature and particle size. Geochim. Cosmochim. Acta, 51: 945–957.

Trolard, F., Bilong, P., Guillet, B. and Herbillon, A.J., 1990. Halloysite–kaolinite–gibbsite–boehmite: a thermodynamical modelisation of equilibria as function of water and dissolved silica activities. In: Y. Noack and D. Nahon (Editors), Geochemistry of the Earth's Surface and of Mineral Formation. Chem. Geol., 84: 294–297 (special issue; extended abstract).